

---

# Why Adam Works Better with $\beta_1 = \beta_2$ : The Missing Gradient Scale Invariance Principle

---

Alberto Fernández-Hernández<sup>1</sup> Cristian Pérez-Corral<sup>1</sup> Jose I. Mestre<sup>2</sup>  
 Manuel F. Dolz<sup>2</sup> Enrique S. Quintana-Ortí<sup>1</sup>

## Abstract

Adam has been at the core of large-scale training for almost a decade, yet a simple empirical fact remains unaccounted for: both validation scores and the qualitative behaviour of the training runs improve when the momentum parameters satisfy  $\beta_1 = \beta_2$ . Some recent studies have reported this pattern, but there is still no explanation for why this choice helps. We show that this choice is closely tied to a structural property that we refer to as *gradient scale invariance*. We formalize this notion and prove that Adam becomes gradient scale invariant of first order if and only if  $\beta_1 = \beta_2$ . This perspective places the balanced regime of Adam in direct alignment with the design principles underlying several recent optimizers that explicitly enforce scale-robust updates. The theory is supported by experiments across vision and language tasks, and across different architectural families, in which rescaling the gradient has a markedly smoother effect on the update when  $\beta_1 = \beta_2$ . Overall, our results offer a coherent explanation for an open question in the behavior of Adam and provide a simple principle that helps guide the design of future optimizers.

## 1. Introduction

Adam (Kingma & Ba, 2015) has played a central role in the training of neural networks ever since it was introduced nearly a decade ago. Its combination of momentum (Sutskever et al., 2013) and per-parameter variance estimation has made it a default choice across architectures and domains, from convolutional networks to LLMs. The original paper proposed the now standard defaults  $\beta_1 = 0.9$  and  $\beta_2 = 0.999$ , and although there have been variations and some task-specific recommendations, such as using

<sup>1</sup>Universitat Politècnica de València, Valencia, Spain

<sup>2</sup>Universitat Jaume I, Castelló de la Plana, Spain. Correspondence to: Alberto Fernández <a.fernandez@upv.es>.

$\beta_2 = 0.95$  in certain LLMs (Touvron et al., 2023), the rationale for keeping two separate momentum parameters and for how they should be related has remained largely unclear.

Recently, some empirical studies driven by Orvieto & Gower (2025) have reported that training can become more stable and accurate when these two parameters are set equal, that is, when  $\beta_1 = \beta_2$ . This observation appears consistently across a range of settings, yet there is no rigorous explanation for why the choice  $\beta_1 = \beta_2$  leads to improved behavior or what aspect of Adam’s dynamics makes this configuration distinctive.

In parallel, many recent optimizers continue to build on ideas introduced by Adam, while incorporating mechanisms that reduce their sensitivity to the magnitude of the gradient. Examples include methods presented by Chen et al. (2023); Liu et al. (2025); Pethick et al. (2025), which are based on normalized updates, sign information, or various forms of clipping. These approaches differ in motivation and formulation, but many of them share the common aim of limiting the influence of gradient scale during training. This trend is becoming increasingly visible in practice and points to the idea that reducing sensitivity to gradient scale is emerging as a desirable property in modern optimizers, even if its connection to the structure of Adam has not yet been clarified.

This work offers a connection between the internal dynamics of Adam and the direction taken by many recent optimizers. The guiding principle is a property that the text refers to as *gradient scale invariance*. Informally, an optimizer is scale invariant if rescaling the gradient by a positive factor leaves the update essentially unchanged. While this property is exact in some simple methods, it is not built into Adam by design, and it is not obvious whether Adam can approximate it. We show that the answer lies in the relation between  $\beta_1$  and  $\beta_2$ . When these two coefficients differ, the update produced by Adam reacts to a change in gradient scale in a way that is linear in the size of the perturbation. When they coincide, the leading dependence disappears and the sensitivity is pushed to second order. This makes the updates far more stable under fluctuations in gradient magnitude, improving both the smoothness of the training dynamics

and the overall behaviour of the method.

Our contributions are as follows:

- We formalize gradient scale invariance and examine how Adam relates to it. Using the continuous-time limit of the algorithm, we analyze how both momentum terms depend on the gradient, and identify when their combined effect removes the first-order dependence on gradient scale in the parameter update. This leads to a clear statement: Adam has gradient scale invariance of first order if and only if  $\beta_1 = \beta_2$ .
- We validate this analysis experimentally. Synthetic examples illustrate how the updates change under multiplicative rescalings of the gradient, and real training runs on a range of vision and language models (NanoGPT on SlimPajama and WikiText, EfficientNet-B0 on TinyImageNet, ResNet18 and ViT-B16 on CIFAR-100, and T5 on SQuAD) show that the norm of the update becomes noticeably smoother when the two parameters coincide.

The rest of the paper is organized as follows. Section 2 reviews related work, touching on theoretical analyses of Adam, recent families of optimizers where invariance plays a central role, and the empirical evidence that points to the regime  $\beta_1 = \beta_2$ . Section 3 introduces gradient scale invariance and sets up the discrete form of Adam. Section 4 presents the Adam flow, develops the analytical expansion that leads to our main result, and illustrates it with synthetic experiments. Section 5 examines the choice of  $\beta$  when  $\beta_1 = \beta_2$  and explores its relation to the number of batches required to train a model. Sections 6 and 7 contain conclusions and limitations.

## 2. Related Work

A substantial body of work has studied Adam (Kingma & Ba, 2015) and related adaptive methods from a theoretical perspective. One line of research develops continuous-time limits that capture a wide class of first-order algorithms as non-autonomous differential equations. In particular, da Silva & Gazeau (2020) derive an Ordinary Differential Equation (ODE) framework that includes AdaGrad (Duchi et al., 2011), RMSProp (Hinton, 2012), Adam and Nesterov (Nesterov, 1983) as special cases, and establish well-posedness and convergence properties of the associated flows. A complementary viewpoint, developed in the optimization literature, emphasizes that Adam often behaves like a normalized or sign-driven method: Balles & Hennig (2018) interpret Adam as combining a sign-based direction with a magnitude modulated by relative variance, while sign methods such as signSGD (Bernstein et al., 2018a) make scale invariance explicit by construction. These perspectives

motivate asking whether, and in which regimes, Adam itself can inherit a principled form of scale robustness.

Another important line is the work of Ma et al. (2022) who study in detail the dynamic behavior of RMSProp and Adam. They observe a characteristic three-phase structure in the loss evolution, consisting of fast initial decrease, an oscillatory regime and late spikes, and interpret these features through a continuous-time limit of Adam that resembles a sign-based gradient flow. Their empirical analysis shows how the choice of hyperparameters, and in particular making  $\beta_1$  and  $\beta_2$  closer, can smooth the dynamics and improve stability in high-accuracy regimes. Related empirical evidence in transformers indicates that Adam’s behavior in low-noise regimes can be closely matched by sign descent with momentum (Kunstner et al., 2023), further supporting the relevance of sign-like mechanisms. However, these works do not isolate the role of gradient scale in the update nor provide a condition that singles out the regime  $\beta_1 = \beta_2$ .

Complementary to these theoretical developments, recent large-scale empirical work has examined how different design choices in Adam affect its performance in transformer-based language models. A key finding of Orvieto & Gower (2025) is that tying the momentum parameters, so that  $\beta_1 = \beta_2$ , preserves the strong performance of Adam while simplified variants based on signed gradients or signed momentum consistently underperform. Their results provide clear empirical support for this choice but leave open the question of why it helps. In particular, they do not relate the behavior of the tied-parameter regime to the role of gradient scale or to any structural property of Adam’s dynamics, which is precisely the gap we address in this work.

Several optimizers have been proposed to improve upon Adam in terms of stability, speed or robustness. The most direct and widely adopted variant is AdamW (Loshchilov & Hutter, 2019), whose strong empirical performance in LLMs stems from decoupling weight decay from the gradient while leaving the core update rules of Adam essentially unchanged. Beyond this refinement, a number of methods introduce genuinely different update mechanisms, often modifying how directions are computed or how step magnitudes are normalized. These approaches typically combine Adam-like momentum with additional normalization or rescaling strategies, and they report more substantial gains over standard Adam in specific regimes. On the Adam-derived side, Lion (Chen et al., 2023) replaces magnitude information by signed updates while retaining an adaptive-momentum strategy, and Shampoo-based methods (Gupta et al., 2018) together with SOAP (Vyas et al., 2025) use Kronecker-structured preconditioning, with the latter in particular applying Adam or Adafactor (Shazeer & Stern, 2018) in the eigenbasis of the preconditioner. Other recent methods such as Muon (Liu et al., 2025) and Scion (Pethick et al.,

2025) move further away from Adam and instead enforce normalized updates directly. Overall, much of the current state-of-the-art optimizers either depend quite intimately on Adam, often still using it on specific parameter subsets, or is explicitly built around normalization mechanisms that reduce the sensitivity of the update to gradient scale, underscoring both the central role of Adam and the importance of scale-robust update rules.

Taken together, these works offer a detailed picture of Adam’s dynamics, provide consistent empirical evidence that tying the momentum parameters can be beneficial, and introduce a growing collection of optimizer variants that reduce sensitivity to gradient magnitude. What is currently missing is a common perspective that links these threads and explains why the regime  $\beta_1 = \beta_2$  is special. The present work addresses this gap by introducing gradient scale invariance as a lens through which these phenomena can be interpreted.

### 3. Gradient Scale Dependence of Adam

This section develops the main theoretical contribution of the paper, formalizing a notion of invariance of a gradient based optimizer with respect to multiplicative changes in gradient scale, and showing how Adam can be related to this property through its underlying dynamics.

#### 3.1. The Gradient Scale Invariance Property

A gradient based optimizer is a rule that generates a sequence of parameters  $(\theta_k)_{k \geq 0} \subset \mathbb{R}^d$  from the gradients

$$\mathbf{g}_k := \nabla f(\theta_k) \in \mathbb{R}^d,$$

via an update of the form

$$\theta_{k+1} = \theta_k - \eta_k \mathbf{R}_k,$$

where  $\eta_k$  represents the learning rate, and the update vector  $\mathbf{R}_k$  is determined by the current gradient  $\mathbf{g}_k$  together with the history of past gradients  $\mathbf{g}_0, \dots, \mathbf{g}_{k-1}$ , typically through auxiliary moment variables.

Intuitively, an optimizer is *gradient scale invariant* if, at a given step  $k$ , its update vector  $\mathbf{R}_k$  does not change when the current gradient  $\mathbf{g}_k$  is replaced by any positive rescaling  $\lambda \mathbf{g}_k$  with  $\lambda > 0$ . In other words, once the internal state of the method at step  $k$  is fixed, only the direction of  $\mathbf{g}_k$  should matter, not its magnitude.

**Definition 3.1.** An optimizer is said to be *gradient scale invariant* if  $\mathbf{R}_k = \tilde{\mathbf{R}}_k$  for every iteration  $k \geq 0$  and every  $\lambda > 0$ , where  $\mathbf{R}_k$  is the update vector corresponding to the gradient  $\mathbf{g}_k$  and  $\tilde{\mathbf{R}}_k$  is the update vector corresponding to the rescaled gradient  $\lambda \mathbf{g}_k$  (with the same internal state at step  $k$ ).

The most immediate example is RPROP (Riedmiller & Braun, 1993), or its mini-batch version signSGD (Bernstein et al., 2018b), where the updates are given by  $\mathbf{R}_k = \text{sign}(\mathbf{g}_k)$  applied coordinate-wise. Optimizer variants that rely primarily on signed information or decouple direction from magnitude, such as Lion, Scion and Muon, can also be viewed as enforcing this property in different approximate forms. In contrast, standard gradient descent uses  $\mathbf{R}_k = \mathbf{g}_k$ , so  $\mathbf{R}_k$  scales linearly with  $\lambda$  under the transformation  $\mathbf{g}_k \mapsto \lambda \mathbf{g}_k$  and is therefore not scale invariant.

For Adam, the situation is more subtle. By construction, Adam combines first and second order moments of the gradient, so the update  $\mathbf{R}_k$  generally changes when  $\mathbf{g}_k$  is rescaled and the definition above is not satisfied. However, a closer look at the dynamics underlying Adam reveals that for suitable choices of  $(\beta_1, \beta_2)$  the optimizer behaves as a nearly scale invariant method. In the rest of this section this connection is made precise by passing to a continuous time description of Adam and analyzing the resulting flow.

#### 3.2. The Adam Flow

The computations of Adam maintain two auxiliary sequences  $(\mathbf{m}_k)_{k \geq 0}$  and  $(\mathbf{v}_k)_{k \geq 0}$  that track first and second order moments of the gradient, and update them as

$$\mathbf{m}_{k+1} = \beta_1 \mathbf{m}_k + (1 - \beta_1) \mathbf{g}_k, \quad (1)$$

$$\mathbf{v}_{k+1} = \beta_2 \mathbf{v}_k + (1 - \beta_2) \mathbf{g}_k^2, \quad (2)$$

where  $\beta_1, \beta_2 \in (0, 1)$  are momentum parameters, and  $\mathbf{g}_k^2$  denotes the coordinate-wise square of  $\mathbf{g}_k$ . The parameter update is given by

$$\theta_{k+1} = \theta_k - \eta_k \frac{\mathbf{m}_{k+1}}{\sqrt{\mathbf{v}_{k+1}} + \varepsilon}, \quad (3)$$

where  $\varepsilon > 0$  is a small stabilization constant. All operations in (1)–(3) are understood coordinate-wise.

In practice, Adam is often used with bias correction of the form  $\mathbf{m}_{k+1}/(1 - \beta_1^{k+1})$  and  $\mathbf{v}_{k+1}/(1 - \beta_2^{k+1})$ , and with  $\varepsilon > 0$ . For clarity, the main exposition considers the raw Adam recurrences (1)–(3), without bias correction and with  $\varepsilon = 0$ . As discussed in Remarks A.4 and A.5 of Appendix A, the analysis extends naturally to the bias-corrected setting and to  $\varepsilon > 0$ , without affecting the structural conclusions.

As previously done in earlier theoretical analyses of adaptive optimization methods (da Silva & Gazeau, 2020; Ma et al., 2022), Adam is interpreted as the time discretization of an underlying continuous-time dynamical system. As is standard in this line of work, we pass to a continuous formulation in order to analyze the resulting flow and its qualitative properties. In the present setting, this perspective allows the study of how the Adam dynamics responds to slow variations in the scale of the gradient, and how this

behavior depends on the relation between the parameters  $\beta_1$  and  $\beta_2$ .

To formalize this viewpoint, consider an explicit time step  $\Delta t > 0$ , define  $t_k = k \Delta t$ , and regard

$$\boldsymbol{\theta}_k \approx \boldsymbol{\theta}(t_k), \quad \mathbf{m}_k \approx \mathbf{m}(t_k),$$

$$\mathbf{v}_k \approx \mathbf{v}(t_k), \quad \mathbf{g}_k \approx \mathbf{g}(t_k) = \nabla f(\boldsymbol{\theta}(t_k)).$$

Consider the discrete momentum coefficients parametrized as

$$\beta_1 = e^{-\Delta t/\tau_1}, \quad \beta_2 = e^{-\Delta t/\tau_2},$$

with relaxation times  $\tau_1, \tau_2 > 0$ , and scale the learning rate as  $\eta = \bar{\eta} \Delta t$  for some  $\bar{\eta} > 0$ . Passing formally to the limit  $\Delta t \rightarrow 0$  in (1)–(3) yields the continuous-time Adam flow

$$\begin{aligned} \tau_1 \mathbf{m}'(t) &= -\mathbf{m}(t) + \mathbf{g}(t), \\ \tau_2 \mathbf{v}'(t) &= -\mathbf{v}(t) + \mathbf{g}(t)^2, \\ \boldsymbol{\theta}'(t) &= -\bar{\eta} \frac{\mathbf{m}(t)}{\sqrt{\mathbf{v}(t)}}, \end{aligned} \tag{4}$$

where  $\mathbf{g}(t) = \nabla f(\boldsymbol{\theta}(t))$  and, again, all operations are taken coordinate-wise.

It will be convenient to isolate the update that drives the parameters. For each coordinate, define

$$\mathbf{R}(t) := \frac{\mathbf{m}(t)}{\sqrt{\mathbf{v}(t)}}, \tag{5}$$

so that the parameter dynamics can be written compactly as

$$\boldsymbol{\theta}'(t) = -\bar{\eta} \mathbf{R}(t).$$

A short derivation of the limit  $\Delta t \rightarrow 0$  underlying (4), together with a clarification of how the relaxation times  $\tau_1, \tau_2$  relate to the discrete coefficients  $\beta_1, \beta_2$ , is provided in Appendix A.1.

### 3.3. Dependence of the Adam Flow on the Gradient

Our objective is to understand how the update  $\mathbf{R}(t)$  depends on the gradient  $\mathbf{g}(t)$ , in particular on the way the magnitude of  $\mathbf{g}(t)$  changes over time, and to show that a first-order scale invariance property holds precisely when  $\tau_1 = \tau_2$ , which corresponds to  $\beta_1 = \beta_2$  in the discrete algorithm.

**Logarithmic scale drift.** A natural way to measure changes in the scale of the gradient is through the logarithmic drift

$$\delta(t) := \frac{d}{dt} \log |\mathbf{g}(t)| = \frac{\mathbf{g}'(t)}{\mathbf{g}(t)}, \tag{6}$$

whenever  $\mathbf{g}(t) \neq 0$ . For each  $i \in \{1, \dots, d\}$ , the quantity  $\delta_i(t)$  is the relative rate of change of  $|g_i(t)|$ : if  $\delta_i(t) \approx 0$ ,

the magnitude of the gradient is essentially constant at time  $t$ , while large values of  $|\delta_i(t)|$  correspond to rapid growth or decay of  $|g_i(t)|$ . Over a short interval of length  $\Delta t$  where  $\delta_i(t)$  is nearly constant, one has that

$$|g_i(t + \Delta t)| \approx |g_i(t)| \exp(\delta_i(t) \Delta t),$$

so  $\delta(t)$  plays the role of a local infinitesimal rescaling rate. This article focuses on the regime where the gradient varies smoothly and its scale drift  $\delta(t)$  is small on the time scales determined by  $\tau_1$  and  $\tau_2$ . In this setting it is natural to treat  $\delta(t)$  as a perturbation parameter and to expand  $\mathbf{m}(t)$ ,  $\mathbf{v}(t)$  and  $\mathbf{R}(t)$  in terms of  $\delta(t)$ .

As in standard analyses of exponential moving averages, one can show that when  $\mathbf{g}(t)$  varies slowly,  $\mathbf{m}(t)$  tracks  $\mathbf{g}(t)$  with a delay of order  $\tau_1$  and  $\mathbf{v}(t)$  tracks  $\mathbf{g}(t)^2$  with a delay of order  $\tau_2$ . During the initial phase of this tracking, however, the transient induced by the initialization of the moments at  $t = t_0$  may blur this behavior. For this reason, the regime  $t - t_0 \gg \max\{\tau_1, \tau_2\}$  is required for initialization effects to become negligible and for the intrinsic tracking dynamics to be observed. The next proposition reformulates this tracking behavior of  $\mathbf{m}(t)$  and  $\mathbf{v}(t)$  in terms of the logarithmic drift  $\delta(t)$ .

**Proposition 3.2** (First-order behavior of  $\mathbf{m}$  and  $\mathbf{v}$ ). *Let  $I = [t_0, t_1]$  be a compact interval and let  $\mathbf{g} : I \rightarrow \mathbb{R}^d$  be a  $C^2$  mapping such that  $g_i(t) \neq 0$  for all  $t \in I$  and all  $i \in \{1, \dots, d\}$ . Let  $\delta(t)$  be defined by (6) and set*

$$\Lambda := \sup_{t \in I} \|\delta(t)\|_\infty, \quad \Lambda' := \sup_{t \in I} \|\delta'(t)\|_\infty.$$

*Let  $\mathbf{m}(t)$  and  $\mathbf{v}(t)$  solve the first two equations of the Adam flow (4). Then, for all  $t \in I$  such that  $t - t_0 \gg \max\{\tau_1, \tau_2\}$ ,*

$$\begin{aligned} \mathbf{m}(t) &= \mathbf{g}(t) \left( 1 - \tau_1 \delta(t) + \mathcal{O}(\Lambda^2 + \Lambda') \right), \\ \mathbf{v}(t) &= \mathbf{g}(t)^2 \left( 1 - 2\tau_2 \delta(t) + \mathcal{O}(\Lambda^2 + \Lambda') \right), \end{aligned}$$

*where the  $\mathcal{O}(\Lambda^2 + \Lambda')$  terms are understood coordinate-wise (equivalently, in  $\|\cdot\|_\infty$ ), uniformly over such times  $t$ , with constants depending only on  $\mathbf{g}$  and on  $\tau_1, \tau_2$ .*

In other words, to first order in the logarithmic drift  $\delta(t)$ ,  $\mathbf{m}(t)$  behaves like  $\mathbf{g}(t)$  corrected by a term  $\tau_1 \delta(t)$ , and  $\mathbf{v}(t)$  behaves like  $\mathbf{g}(t)^2$  corrected by a term  $2\tau_2 \delta(t)$ . Precise estimates, including explicit bounds on the remainder terms and a proof of Proposition 3.2, are given in Proposition A.2 of Appendix A.

Now, Proposition 3.2 permits to describe how the logarithmic drift  $\delta(t)$  affects the update  $\mathbf{R}(t)$ . On an interval where  $\mathbf{g}(t)$  does not change sign,  $\mathbf{m}(t)$  and  $\sqrt{\mathbf{v}(t)}$  can be written in terms of  $\mathbf{g}(t)$  and  $\delta(t)$ , and then expand the ratio. The next theorem gives the resulting first-order behavior.

**Theorem 3.3** (First-order expansion of the normalized update). *Let  $I = [t_0, t_1]$  and  $\mathbf{g} : I \rightarrow \mathbb{R}^d$  be a  $C^2$  mapping, and assume that  $|g_i(t)| \geq g_{\min,i} > 0$  for all  $t \in I$  and all  $i \in \{1, \dots, d\}$ . With  $\Lambda$  and  $\Lambda'$  as above, there exists  $\varepsilon_0 > 0$  such that, if  $\Lambda \leq \varepsilon_0$ , then for all  $t \in I$  such that  $t - t_0 \gg \max\{\tau_1, \tau_2\}$ ,*

$$\mathbf{R}(t) = \text{sign}(\mathbf{g}(t)) \left( 1 + (\tau_2 - \tau_1) \delta(t) + \mathcal{O}(\Lambda^2 + \Lambda') \right),$$

where  $\text{sign}(\mathbf{g}(t))$  is taken coordinate-wise, and the remainder is uniform (in  $\|\cdot\|_\infty$ ) over such times  $t$ , with constants depending only on  $\mathbf{g}$  and on  $\tau_1, \tau_2$ .

*Remark 3.4.* The transient regimes in Proposition 3.2 and Theorem 3.3 reflect only the initialization of the moment estimates and does not restrict generality; once the moments reach their natural tracking regime, the first-order behavior governs the full training dynamics.

A detailed proof of Theorem 3.3, together with additional comments on the underlying regularity assumptions, is provided in Theorem A.3 of Appendix A. Theorem 3.3 shows that, in the regime where the gradient magnitude changes slowly, the normalized Adam update tracks  $\text{sign}(\mathbf{g}(t))$  corrected by a term  $(\tau_2 - \tau_1)\delta(t)$ .

### 3.4. First Order Gradient Scale Invariance when

$$\beta_1 = \beta_2$$

The expansion obtained in Theorem 3.3 already reveals a clear pattern: at leading order, Adam behaves like a sign-based method, and deviations from this behavior are governed by the first-order term  $(\tau_2 - \tau_1)\delta(t)$ . To capture this phenomenon, it is natural to relax the notion of gradient scale invariance and allow controlled violations that appear only at higher order in the quantity  $\delta(t)$ .

**Definition 3.5.** Consider the continuous-time interpretation of an optimizer, with update  $\mathbf{R}(t)$  and gradient  $\mathbf{g} : \mathbb{R} \rightarrow \mathbb{R}^d$  being a  $C^k$  mapping along a trajectory, with  $\mathbf{g}(t) \neq \mathbf{0}$  on  $I$ . Let  $\delta(t)$  be the logarithmic scale drift defined in (6), and let  $\Lambda$  and  $\Lambda'$  be the corresponding uniform bounds over  $I$ , as in Proposition 3.2. The optimizer is *gradient scale invariant of first order* along this trajectory if there exists  $\varepsilon_0 > 0$  and a gradient scale invariant optimizer in the sense of Definition 3.1 with update  $\mathbf{R}^{\text{inv}}(t)$  such that, whenever  $\Lambda \leq \varepsilon_0$  and for every  $t \in I$  satisfying  $t - t_0 \gg \max\{\tau_1, \tau_2\}$ , one has that

$$\mathbf{R}(t) = \mathbf{R}^{\text{inv}}(t) + \mathcal{O}(\Lambda^2 + \Lambda'),$$

where the remainder is uniform in  $t$  (in  $\|\cdot\|_\infty$ ) over such times.

Intuitively, an optimizer is gradient scale invariant to first order when, once the initialization transient has decayed and the logarithmic scale drift  $\delta(t)$  remains small, its update becomes indistinguishable from that of a truly scale invariant

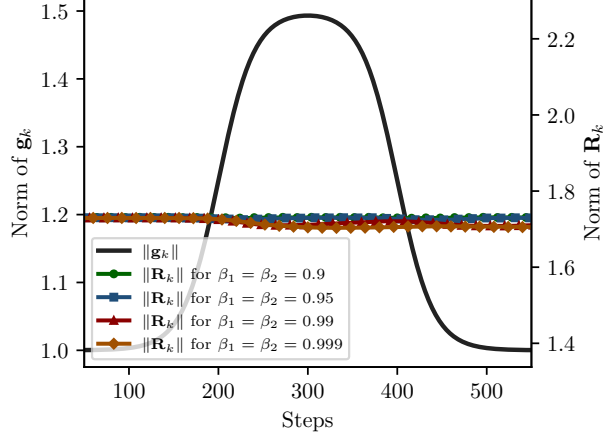


Figure 1. Evolution of  $\|\mathbf{R}_k\|$  in Adam for  $\beta_1 = \beta_2$ .

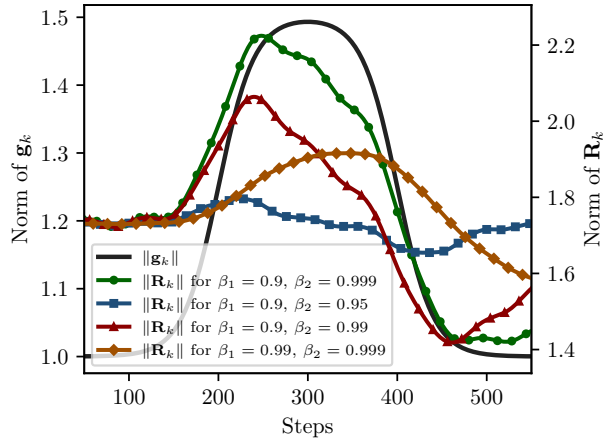


Figure 2. Evolution of  $\|\mathbf{R}_k\|$  in Adam for  $\beta_1 \neq \beta_2$ .

optimizer up to second order effects. In this regime, any residual dependence on the gradient scale is dominated by terms of order  $\mathcal{O}(\Lambda^2 + \Lambda')$ , so that scale enters only beyond first order.

A direct consequence of Theorem 3.3 is the following corollary, which characterizes this property for the Adam optimizer.

**Corollary 3.6** (First-order gradient scale invariance of Adam). *The Adam flow is gradient scale invariant of first order if and only if  $\tau_1 = \tau_2$ . In discrete time, this corresponds to  $\beta_1 = \beta_2$ .*

Although the analysis is local in the logarithmic scale drift, this is analogous to standard local expansions in dynamical systems: the cancellation of the first-order scale term at each time instant accumulates over training and manifests globally as smoother update trajectories. The empirical results in Section 4 show that this local structural property translates into persistent stability across long training horizons.

Figures 1 and 2 present a simple synthetic experiment in which we alter the scale of a one-dimensional gradient signal and record the corresponding update  $\mathbf{R}(t)$  for different choices of  $(\beta_1, \beta_2)$ . As predicted by the theory, we observe in Figure 1 that the norm of  $\mathbf{R}(t)$  remains remarkably stable when  $\beta_1 = \beta_2$ , showing only minor second-order deviations. When  $\beta_1 \neq \beta_2$  in Figure 2, the update attempts to compensate for the scale change but nonetheless exhibits a clear first-order sensitivity consistent with the theory.

These findings shed light on a phenomenon repeatedly reported in recent experimental studies, including [Orvieto & Gower \(2025\)](#) and [Ma et al. \(2022\)](#): Adam consistently performs better and more stably when  $\beta_1 = \beta_2$ . Our analysis shows that this is not an empirical curiosity, but the visible trace of a deeper structural alignment. When the two

time scales coincide, Adam becomes, to first order, gradient scale invariant, placing it in the same conceptual class as several modern state-of-the-art optimizers. Methods such as Lion, Muon and Scion are explicitly designed around this principle, yet our results reveal that the same ingredient was already latent inside Adam, and emerges precisely in the balanced regime  $\beta_1 = \beta_2$ . In this way, the theory closes a long-standing gap between two previously disconnected lines of evidence: the empirical success of balanced Adam and the deliberate scale-invariant design of recent optimizers. It identifies gradient scale invariance as a unifying mechanism behind their stability and efficiency, and explains why this specific configuration of Adam naturally inherits these desirable properties.

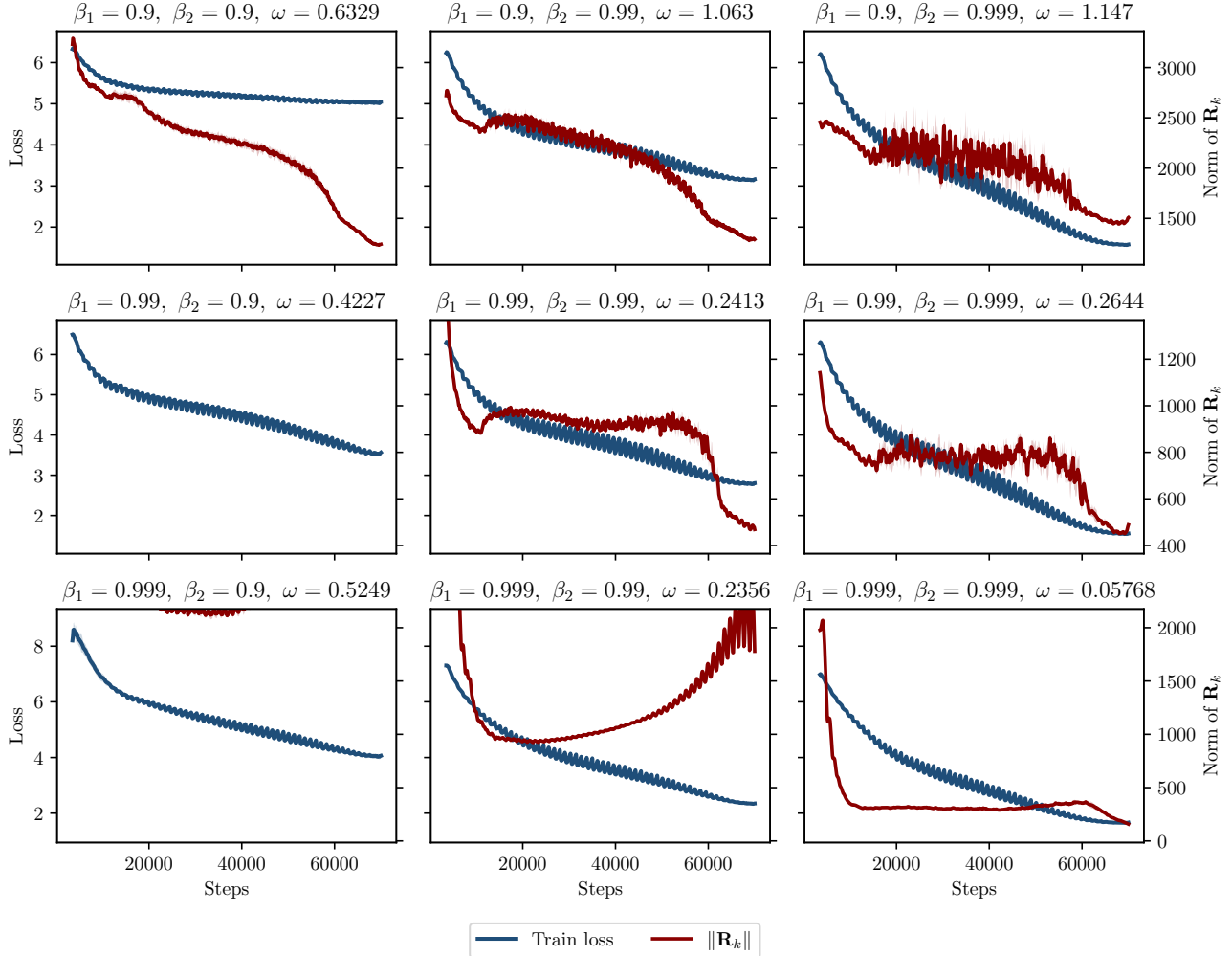


*Figure 3.* Training dynamics for NanoGPT on WikiText. Each panel shows the evolution of the training loss (left axis) and the norm of the update  $\mathbf{R}_k$  (right axis) for a fixed pair  $(\beta_1, \beta_2)$ . Rows correspond to fixed  $\beta_1$  and columns to varying  $\beta_2$ , with identical axis scales within each row. Curves show the seed-averaged dynamics after exponential smoothing (window of 200 steps), with shaded regions indicating one standard deviation across seeds; the oscillation metric  $\omega$  is reported in the title. Configurations with  $\beta_1 = \beta_2$  exhibit systematically smoother update norms, while off-diagonal choices lead to increased oscillations.

## 4. Effect of the First Order Gradient Scale Invariance in Training

The theoretical analysis of the previous section shows that Adam is gradient scale invariant to first order if and only if the momentum parameters satisfy  $\beta_1 = \beta_2$ . While this property may appear purely structural, it has direct and observable consequences in practical training dynamics. In particular, first-order scale invariance implies that the update vector  $\mathbf{R}_k$  is less sensitive to variations in the norm of the gradient and is instead driven primarily by its direction. As a result, not all changes in  $\mathbf{g}_k$  have the same impact on the update, leading to smoother trajectories and increased stability during training.

While most empirical studies focus on loss or accuracy, our theory predicts a direct effect on the stability of the update itself. We therefore study the dynamics of the update norm  $\|\mathbf{R}_k\|$ , which directly reflects sensitivity to gradient scale, and quantify oscillation  $\omega$  as the average absolute variation of  $\|\mathbf{R}_k\|$  between consecutive steps after applying an exponential moving average with a window of 200 steps to suppress high-frequency stochastic noise. Robustness to alternative windows and to different definitions of the oscillation metric is reported in Appendix B.

Experiments are conducted on six network–dataset pairs

covering both vision and language tasks: NanoGPT on SlimPajama and WikiText, EfficientNet-B0 on TinyImageNet, ResNet18 and ViT-B16 on CIFAR-100, and T5 on SQuAD. For each pair, we train the model using Adam or AdamW over a  $3 \times 3$  grid of momentum parameters  $\beta_1, \beta_2 \in \{0.9, 0.99, 0.999\}$ . All configurations are repeated with three different random seeds, except for NanoGPT on SlimPajama, where a single seed is used due to computational constraints; see Appendix C for full implementation and training details.

Figure 3 illustrates representative training runs for NanoGPT on WikiText. Each panel shows the evolution of the training loss and the norm  $\|\mathbf{R}_k\|$ , displayed on the left and right vertical axes. Within each row,  $\beta_1$  is fixed and the three columns correspond to different values of  $\beta_2$ ; the horizontal and vertical scales are kept identical across a row to allow direct comparison. The title of each panel reports the corresponding values of  $(\beta_1, \beta_2)$  together with the oscillation metric  $\omega$ . When  $\beta_1 > \beta_2$ , Adam tends to exhibit explosive behavior, causing  $\|\mathbf{R}_k\|$  to take values far outside the scale of the other configurations in the same row. In such cases the curve may extend beyond the plotting range; nevertheless, the associated value of  $\omega$ , reported in the title, captures this instability quantitatively.

The qualitative pattern is immediate. For a fixed  $\beta_1$ , the

*Table 1.* Oscillation values  $\omega(\beta_1, \beta_2)$ , averaged over seeds when applicable, for all network–dataset pairs. For each fixed  $\beta_1$ , the minimum oscillation within the row is highlighted in bold. The *Rate* column reports the fraction of rows (fixing  $\beta_1$  and seed) in which the minimizing  $\beta_2$  coincides with  $\beta_1$ . The last column reports the *p*-value of a one-sided exact binomial test assessing whether the diagonal is selected more often than expected under a uniform null model.

Exp.	Network	Dataset	$\beta_1$	$\omega(\beta_1, \beta_2)$			Rate	<i>p</i> -value
				$\beta_2 = 0.9$	$\beta_2 = 0.99$	$\beta_2 = 0.999$		
1	NanoGPT	WikiText	0.9	<b>0.6329</b>	1.063	1.147	100%	$5.08 \times 10^{-5}$
			0.99	0.4227	<b>0.2413</b>	0.2644		
			0.999	0.5249	0.2356	<b>0.05768</b>		
2	EfficientNet-B0	TinyImageNet	0.9	<b>0.08169</b>	0.1869	0.217	100%	$5.08 \times 10^{-5}$
			0.99	$3.312 \times 10^5$	<b>0.01430</b>	0.03121		
			0.999	$4.918 \times 10^6$	$2.466 \times 10^5$	<b>0.002931</b>		
3	T5	SQuAD	0.9	0.3902	<b>0.3455</b>	0.5714	77.8%	0.00828
			0.99	1.203	<b>0.03733</b>	0.06729		
			0.999	1.731	1.137	<b>0.003777</b>		
4	ResNet18	CIFAR-100	0.9	<b>0.05120</b>	0.09750	0.09028	75%	$3.92 \times 10^{-4}$
			0.99	0.5414	<b>0.01008</b>	0.01963		
			0.999	0.9214	0.1339	<b>0.004201</b>		
5	NanoGPT	SlimPajama	0.9	<b>0.4988</b>	0.8467	1.169	100%	0.0370
			0.99	0.3404	<b>0.1947</b>	0.2489		
			0.999	0.3372	0.07359	<b>0.05921</b>		
6	ViT-B16	CIFAR-100	0.9	<b>0.2925</b>	0.6410	0.6777	100%	$5.08 \times 10^{-5}$
			0.99	356.3	<b>0.07104</b>	0.09244		
			0.999	NaN	204.2	<b>0.0735</b>		

oscillation of  $\|\mathbf{R}_k\|$  increases as  $\beta_2$  moves away from  $\beta_1$ , while the diagonal configuration  $\beta_1 = \beta_2$  consistently produces the smoothest update trajectory within each row. This behavior aligns with the theoretical prediction: when the two time scales coincide, the first-order dependence of  $\mathbf{R}_k$  on gradient scale vanishes, thus making  $\|\mathbf{R}_k\|$  more stable. The corresponding plots for the remaining experiments are reported in Appendix B for space reasons, and exhibit the same qualitative behavior as in Figure 3.

Table 1 summarizes the oscillation values  $\omega = \omega(\beta_1, \beta_2)$  across all experiments. For each fixed  $\beta_1$ , the minimum oscillation is systematically attained on the diagonal  $\beta_2 = \beta_1$ . This trend is further quantified by the *Rate* column, which reports the fraction of cases, fixing  $\beta_1$  and the random seed, in which the minimizing  $\beta_2$  coincides with  $\beta_1$ .

To assess the statistical significance of this effect, we perform a simple hypothesis test. Fixing the network, dataset,  $\beta_1$ , and random seed, we identify the value of  $\beta_2$  that minimizes  $\omega$ . Under the null hypothesis that no structural alignment is present, this minimizing  $\beta_2$  is uniformly distributed among the 3 tested values, so that  $\mathbb{P}(\beta_2^* = \beta_1) = 1/3$ . We record whether the diagonal is selected and aggregate this indicator over all evaluated rows, obtaining a count  $K$  over  $N$  trials. Under the null,  $K$  follows a  $\text{Binomial}(N, 1/3)$  distribution. Statistical significance is quantified reporting the probability of observing at least  $K$  diagonal selections. The resulting  $p$ -values, reported in the last column of Table 1, strongly favor the alternative hypothesis in all settings. The few values closer to the conventional threshold arise precisely in configurations with fewer independent seeds, where statistical power is reduced. Overall, the evidence supports the same conclusion: in the explored regime, the diagonal  $\beta_1 = \beta_2$  minimizes the oscillation of  $\|\mathbf{R}_k\|$ .

These results thus demonstrate that the first-order gradient scale invariance identified in the continuous-time analysis leaves a clear and measurable imprint in practical training. The regime  $\beta_1 = \beta_2$  is not merely a convenient hyperparameter choice, but the configuration in which Adam exhibits the most stable update dynamics, in direct agreement with the theoretical characterization.

## 5. Conclusions

Recent empirical studies, most notably the extensive analysis of (Orvieto & Gower, 2025), have consistently observed that Adam exhibits its most stable and accurate behavior when the momentum parameters are tied,  $\beta_1 = \beta_2$ . While this regime has been broadly validated across architectures and tasks, a principled explanation for its special role has remained elusive. The aim of this work has been to uncover the structural mechanism responsible for this behavior.

By analyzing the continuous-time limit of Adam, we show

that the balanced regime is characterized by a precise invariance property: Adam becomes gradient scale invariant to first order if and only if  $\beta_1 = \beta_2$ . In this setting, the leading dependence of the update on gradient magnitude vanishes, leaving dynamics driven primarily by directional information. This provides a direct theoretical explanation for the enhanced stability observed in practice.

This viewpoint also places balanced Adam within a broader landscape of modern optimizers. Recent methods such as Muon, Scion, and related approaches explicitly aim to suppress sensitivity to gradient scale in their update rules. Our results reveal that the same principle is already embedded within Adam and naturally emerges in its empirically optimal regime, thereby unifying classical adaptive optimization with contemporary scale-robust designs.

Empirically, this mechanism manifests as a systematic reduction in oscillations of the update norm across diverse models and datasets. The observed smoothing of training dynamics provides a concrete signature of first-order gradient scale invariance in real optimization trajectories.

Together, these findings explain why the choice  $\beta_1 = \beta_2$  consistently yields the most reliable behavior in Adam and highlight gradient scale invariance as a central structural feature underlying stable adaptive optimization. More broadly, they suggest that robustness to gradient rescaling is not merely a heuristic improvement, but a fundamental design principle for future optimizers.

## Future Work

An immediate direction for future work concerns the choice of the common momentum parameter in the balanced regime  $\beta_1 = \beta_2$ . While recent empirical studies suggest that values around  $\beta \approx 0.95$  can perform well in practice, this choice is not universal and its optimality remains poorly understood. A principled characterization of the optimal  $\beta$  as a function of factors such as gradient noise, batch size, or training horizon could further simplify the use of Adam and related methods by effectively removing a hyperparameter.

A second direction is to extend the notion of gradient scale invariance beyond first order. Our analysis identifies the cancellation of the leading-order scale-dependent term as the key mechanism underlying the stability of balanced Adam. Understanding whether higher-order invariance can be achieved, or approximated, may provide additional insight into the design of adaptive methods with even stronger stability properties.

More broadly, the perspective developed in this work suggests that robustness to gradient rescaling is not merely a desirable side effect, but a structural principle that can guide the analysis and development of future optimizers.

## Impact Statement

This work contributes to a clearer understanding of the dynamics of Adam and related adaptive optimizers. Its impact lies in two directions. First, by clarifying which scale-related properties are desirable in an optimizer, our analysis aims to support future theoretical progress toward methods that converge faster, use memory more efficiently, and behave more robustly during training. Second, our study provides complementary theoretical insight and practical guidance on how the momentum parameters in Adam and AdamW should be chosen, identifying the regime  $\beta_1 = \beta_2$  as principled and offering evidence for appropriate values of the remaining hyperparameter. Overall, the goal is to inform the development of training procedures that use computational resources more effectively, helping make large-scale deep learning models more accessible and sustainable.

## Acknowledgements

This research was funded by the projects PID2023-146569NB-C21 and PID2023-146569NB-C22 supported by MICIU/AEI/10.13039/501100011033 and ERDF/UE. Alberto Fernández-Hernández was supported by the predoctoral grant PREP2023-001826 supported by MICIU/AEI/10.13039/501100011033 and ESF+. Cristian Pérez-Corral received support from the *Conselleria de Educación, Cultura, Universidades y Empleo* (reference CIACIF/2024/412) through the European Social Fund Plus 2021–2027 (FSE+) program of the *Comunitat Valenciana*. Jose I. Mestre was supported by the predoctoral grant ACIF/2021/281 of the *Generalitat Valenciana*. Manuel F. Dolz was supported by the Plan Gen-T grant CIDEXG/2022/13 of the *Generalitat Valenciana*.

## References

Balles, L. and Hennig, P. Dissecting Adam: The sign, magnitude and variance of stochastic gradients. In Dy, J. and Krause, A. (eds.), *Proceedings of the 35th International Conference on Machine Learning*, volume 80 of *Proceedings of Machine Learning Research*, pp. 404–413. PMLR, 10–15 Jul 2018. URL <https://proceedings.mlr.press/v80/balles18a.html>.

Bernstein, J., Wang, Y.-X., Azizzadenesheli, K., and Anandkumar, A. signSGD: Compressed optimisation for non-convex problems. In Dy, J. and Krause, A. (eds.), *Proceedings of the 35th International Conference on Machine Learning*, volume 80 of *Proceedings of Machine Learning Research*, pp. 560–569. PMLR, 10–15 Jul 2018a. URL <https://proceedings.mlr.press/v80/bernstein18a.html>.

Bernstein, J., Wang, Y.-X., Azizzadenesheli, K., and Anandkumar, A. signsdg: Compressed optimisation for non-convex problems. In Dy, J. and Krause, A. (eds.), *Proceedings of the 35th International Conference on Machine Learning*, volume 80 of *Proceedings of Machine Learning Research*, pp. 560–569. PMLR, 2018b. URL <https://proceedings.mlr.press/v80/bernstein18a.html>.

Chen, X., Liang, C., Huang, D., Real, E., Wang, K., Pham, H., Dong, X., Luong, T., Hsieh, C.-J., Lu, Y., and Le, Q. V. Symbolic discovery of optimization algorithms. In *Proceedings of the 37th International Conference on Neural Information Processing Systems*, NIPS ’23, Red Hook, NY, USA, 2023. Curran Associates Inc. URL <https://dl.acm.org/doi/10.5555/366122.3668262>.

da Silva, A. B. and Gazeau, M. A general system of differential equations to model first-order adaptive algorithms. *Journal of Machine Learning Research*, 21(129):1–42, 2020. URL <http://jmlr.org/papers/v21/18-808.html>.

Duchi, J., Hazan, E., and Singer, Y. Adaptive subgradient methods for online learning and stochastic optimization. *Journal of Machine Learning Research*, 12(61):2121–2159, 2011. URL <http://jmlr.org/papers/v12/duchi11a.html>.

Fernández-Hernández, A., Mestre, J. I., Dolz, M. F., Duato, J., and Quintana-Ortí, E. S. Sinusoidal initialization, time for a new start. In *Advances in Neural Information Processing Systems*, 2025. URL <https://openreview.net/forum?id=FGliQVcrDZ>.

Gupta, V., Koren, T., and Singer, Y. Shampoo: Preconditioned stochastic tensor optimization. In Dy, J. and Krause, A. (eds.), *Proceedings of the 35th International Conference on Machine Learning*, volume 80 of *Proceedings of Machine Learning Research*, pp. 1842–1850. PMLR, 10–15 Jul 2018. URL <https://proceedings.mlr.press/v80/gupta18a.html>.

Hinton, G. E. Neural networks for machine learning, lecture 6a: Overview of mini-batch gradient descent. Coursera video lecture, University of Toronto, 2012. [https://www.cs.toronto.edu/~tijmen/csc321/slides/lecture\\_slides\\_lec6.pdf](https://www.cs.toronto.edu/~tijmen/csc321/slides/lecture_slides_lec6.pdf).

Kingma, D. P. and Ba, J. Adam: A method for stochastic optimization. In *International Conference on Learning Representations (ICLR)*, 2015. URL <https://arxiv.org/abs/1412.6980>.

Kunstner, F., Trager, M., Hosseini, R., Nakkiran, P., and Srebro, N. Noise is not the main factor behind

the gap between SGD and Adam on transformers, but sign descent might be. In *Proceedings of the International Conference on Learning Representations (ICLR)*, 2023. URL <https://openreview.net/forum?id=a65YK0cqH8g>.

Liu, J., Su, J., Yao, X., Jiang, Z., Lai, G., Du, Y., Qin, Y., Xu, W., Lu, E., Yan, J., Chen, Y., Zheng, H., Liu, Y., Liu, S., Yin, B., He, W., Zhu, H., Wang, Y., Wang, J., Dong, M., Zhang, Z., Kang, Y., Zhang, H., Xu, X., Zhang, Y., Wu, Y., Zhou, X., and Yang, Z. Muon is scalable for llm training, 2025. URL <https://arxiv.org/abs/2502.16982>.

Loshchilov, I. and Hutter, F. Decoupled weight decay regularization. In *International Conference on Learning Representations (ICLR)*, 2019.

Ma, C., Wu, L., and E, W. A qualitative study of the dynamic behavior for adaptive gradient algorithms. In Bruna, J., Hesthaven, J., and Zdeborova, L. (eds.), *Proceedings of the 2nd Mathematical and Scientific Machine Learning Conference*, volume 145 of *Proceedings of Machine Learning Research*, pp. 671–692. PMLR, 16–19 Aug 2022. URL <https://proceedings.mlr.press/v145/ma22a.html>.

Nesterov, Y. E. A method of solving a convex programming problem with convergence rate  $o(1/k^2)$ . *Doklady Akademii Nauk SSSR*, 269(3):543–547, 1983. URL <http://mi.mathnet.ru/dan46009>.

Orvieto, A. and Gower, R. M. In search of Adam’s secret sauce. In *Advances in Neural Information Processing Systems*, 2025. URL <https://openreview.net/forum?id=CH72XyZs4y>.

Pethick, T., Xie, W., Antonakopoulos, K., Zhu, Z., Silverti-Falls, A., and Cevher, V. Training deep learning models with norm-constrained lmos. In Singh, A., Fazel, M., Hsu, D., Lacoste-Julien, S., Berkenkamp, F., Maharaj, T., Wagstaff, K., and Zhu, J. (eds.), *Proceedings of the 42nd International Conference on Machine Learning*, volume 267 of *Proceedings of Machine Learning Research*, pp. 49069–49104. PMLR, 2025. URL <https://proceedings.mlr.press/v267/pethick25a.html>.

Riedmiller, M. and Braun, H. A direct adaptive method for faster backpropagation learning: the rprop algorithm. In *IEEE International Conference on Neural Networks*, pp. 586–591 vol.1, 1993. doi: 10.1109/ICNN.1993.298623. URL <https://ieeexplore.ieee.org/document/298623>.

Shazeer, N. and Stern, M. Adafactor: Adaptive learning rates with sublinear memory cost. In Dy, J. and Krause, A. (eds.), *Proceedings of the 35th International Conference on Machine Learning*, volume 80 of *Proceedings of Machine Learning Research*, pp. 4596–4604. PMLR, 2018. URL <https://proceedings.mlr.press/v80/shazeer18a.html>.

Sutskever, I., Martens, J., Dahl, G., and Hinton, G. E. On the importance of initialization and momentum in deep learning. In Dasgupta, S. and McAllester, D. (eds.), *Proceedings of the 30th International Conference on Machine Learning*, volume 28 of *Proceedings of Machine Learning Research*, pp. 1139–1147, Atlanta, Georgia, USA, 2013. PMLR. URL <https://proceedings.mlr.press/v28/sutskever13.html>.

Touvron, H., Lavril, T., Izacard, G., Martinet, X., Lachaux, M.-A., Lacroix, T., Rozière, B., Goyal, N., Hambro, E., Azhar, F., Rodriguez, A., Joulin, A., Grave, E., and Lample, G. Llama: Open and efficient foundation language models, February 2023. URL <http://arxiv.org/abs/2302.13971>. arXiv:2302.13971 [cs.CL].

Vyas, N., Morwani, D., Zhao, R., Shapira, I., Brandfonbrener, D., Janson, L., and Kakade, S. M. SOAP: Improving and stabilizing Shampoo using Adam for language modeling. In *International Conference on Learning Representations*, 2025. URL <https://openreview.net/forum?id=IDxZhXrpNf>. ICLR 2025, Poster.

## A. Technical Details for the Adam Flow

This appendix collects the technical material that supports the statements in the main text. It opens with a short derivation of the continuous-time Adam flow from the discrete updates, clarifying the role of the relaxation times  $\tau_1$  and  $\tau_2$ . It then turns to a detailed analysis of the behavior of the first and second moments  $\mathbf{m}(t)$  and  $\mathbf{v}(t)$ , and of their relation to the logarithmic scale drift  $\delta(t)$ .

### A.1. From Discrete Adam to the Continuous-time Flow

This first section justifies the continuous-time system (4) and clarifies the role of the parameters  $\beta_1, \beta_2$  and  $\tau_1, \tau_2$ .

Consider, for simplicity, a single coordinate of Adam's first moment. The discrete update is

$$m_{k+1} = \beta_1 m_k + (1 - \beta_1) g_k, \quad t_k = k \Delta t.$$

Assuming that  $m_k \approx m(t_k)$  and  $g_k \approx g(t_k)$  for smooth functions  $m(t)$  and  $g(t)$ , the forward difference can be written as

$$\frac{m_{k+1} - m_k}{\Delta t} = \frac{\beta_1 - 1}{\Delta t} m_k + \frac{1 - \beta_1}{\Delta t} g_k.$$

When  $\beta_1$  is close to 1, as is the case in practical implementations of Adam, a relaxation time  $\tau_1 > 0$  may be introduced through the asymptotic relation

$$1 - \beta_1 = \frac{\Delta t}{\tau_1} + o(\Delta t).$$

This implies

$$\frac{\beta_1 - 1}{\Delta t} = -\frac{1}{\tau_1} + o(1), \quad \frac{1 - \beta_1}{\Delta t} = \frac{1}{\tau_1} + o(1).$$

Letting  $\Delta t \rightarrow 0$  while keeping  $\tau_1$  fixed, the difference quotient converges to  $m'(t)$ , yielding

$$\tau_1 m'(t) = -m(t) + g(t),$$

which recovers the first equation in (4). The same argument applied to

$$v_{k+1} = \beta_2 v_k + (1 - \beta_2) g_k^2$$

gives

$$\tau_2 v'(t) = -v(t) + g(t)^2.$$

An important point is that the correspondence between  $\beta$  and  $\tau$  is not unique. Any relation of the form

$$\beta(\tau, \Delta t) = 1 - \frac{\Delta t}{\tau} + o(\Delta t)$$

leads to the same limiting differential equation. The exponential parametrization

$$\beta = e^{-\Delta t/\tau}$$

adopted in the main text is a convenient choice, as it enforces  $0 < \beta < 1$  for all  $\Delta t > 0$  and makes the small- $\Delta t$  behavior explicit, but it is by no means the only one compatible with the continuous-time limit.

This perspective also clarifies the interpretation of the parameters. Although one may write  $\beta = \beta(\tau, \Delta t)$  through relations such as  $\beta = e^{-\Delta t/\tau}$ , in Adam the quantities  $\beta_1$  and  $\beta_2$  are the primitive, fixed hyperparameters of the algorithm. The corresponding time scales  $\tau_1$  and  $\tau_2$  are therefore defined implicitly from  $(\beta, \Delta t)$  and represent the effective relaxation times of the associated continuous-time system. In this sense,  $\tau_1$  and  $\tau_2$  characterize the limiting continuous dynamics, whereas  $\beta_1$  and  $\beta_2$  are the discrete parameters appearing in Adam's updates.

## A.2. First Order Expansions for the Moments $\mathbf{m}(t)$ and $\mathbf{v}(t)$

Recall that the Adam flow is given by

$$\begin{aligned}\tau_1 \mathbf{m}'(t) &= -\mathbf{m}(t) + \mathbf{g}(t), \\ \tau_2 \mathbf{v}'(t) &= -\mathbf{v}(t) + \mathbf{g}(t)^2, \\ \boldsymbol{\theta}'(t) &= -\bar{\eta} \frac{\mathbf{m}(t)}{\sqrt{\mathbf{v}(t)}},\end{aligned}\tag{7}$$

where the operations are understood coordinate-wise, and that the logarithmic scale drift is defined by

$$\delta_i(t) := \frac{d}{dt} \log |g_i(t)| = \frac{g'_i(t)}{g_i(t)},\tag{8}$$

for each coordinate  $i$ , whenever  $g_i(t) \neq 0$ . We write  $\boldsymbol{\delta}(t) = (\delta_1(t), \dots, \delta_d(t))$ .

To streamline the proof of Proposition 3.2, it is convenient to isolate a basic tracking fact for the scalar linear ODE  $\tau x' = -x + y(t)$ : the state  $x(t)$  follows the signal  $y(t)$  with a characteristic lag of order  $\tau$ , and the resulting error is controlled by how rapidly  $y(t)$  varies.

**Lemma A.1** (Tracking a slowly varying signal). *Let  $I = [t_0, t_1]$  be a compact interval and let  $y \in C^2(I, \mathbb{R})$ . For fixed  $\tau > 0$ , let  $x : I \rightarrow \mathbb{R}$  solve*

$$\tau x'(t) = -x(t) + y(t),$$

for  $t \in I$ , with initial condition  $x(t_0) = x_0$ . Set  $M := \sup_{t \in I} |y''(t)|$ . Then, for all  $t \in I$ ,

$$x(t) = y(t) - \tau y'(t) + r(t),$$

where the remainder  $r(t)$  satisfies

$$|r(t)| \leq |x_0 - y(t_0) + \tau y'(t_0)| e^{-(t-t_0)/\tau} + \tau^2 M.$$

*Proof.* The solution of  $\tau x'(t) = -x(t) + y(t)$  with initial condition  $x(t_0) = x_0$  follows from the variation of constants formula and reads

$$x(t) = e^{-(t-t_0)/\tau} x_0 + \int_{t_0}^t K(t, s) y(s) ds$$

with

$$K(t, s) := \frac{1}{\tau} e^{-(t-s)/\tau},$$

Notice that

$$\partial_s K(t, s) = \frac{1}{\tau^2} e^{-(t-s)/\tau} = \frac{1}{\tau} K(t, s),$$

so that an integration by parts yields

$$\begin{aligned}\int_{t_0}^t K(t, s) y(s) ds &= \tau K(t, t) y(t) - \tau K(t, t_0) y(t_0) - \tau \int_{t_0}^t K(t, s) y'(s) ds \\ &= y(t) - e^{-(t-t_0)/\tau} y(t_0) - \tau \int_{t_0}^t K(t, s) y'(s) ds.\end{aligned}$$

Substituting the expression of  $x(t)$  implies that

$$x(t) = e^{-(t-t_0)/\tau} x_0 + y(t) - e^{-(t-t_0)/\tau} y(t_0) - \tau \int_{t_0}^t K(t, s) y'(s) ds.$$

An integration by parts once again to the term involving  $y'$  yields

$$\begin{aligned}\tau \int_{t_0}^t K(t, s) y'(s) ds &= \tau^2 K(t, t) y'(t) - \tau^2 K(t, t_0) y'(t_0) - \tau^2 \int_{t_0}^t K(t, s) y''(s) ds \\ &= \tau y'(t) - \tau e^{-(t-t_0)/\tau} y'(t_0) - \tau^2 \int_{t_0}^t K(t, s) y''(s) ds.\end{aligned}$$

Combining the expressions obtained above, it follows that

$$\begin{aligned} x(t) &= e^{-(t-t_0)/\tau} x_0 + y(t) - e^{-(t-t_0)/\tau} y(t_0) - \tau y'(t) + \tau e^{-(t-t_0)/\tau} y'(t_0) + \tau^2 \int_{t_0}^t K(t,s) y''(s) ds \\ &= y(t) - \tau y'(t) + (x_0 - y(t_0) + \tau y'(t_0)) e^{-(t-t_0)/\tau} + \tau^2 \int_{t_0}^t K(t,s) y''(s) ds, \end{aligned}$$

which yields the desired representation with

$$r(t) = (x_0 - y(t_0) + \tau y'(t_0)) e^{-(t-t_0)/\tau} + \tau^2 \int_{t_0}^t K(t,s) y''(s) ds.$$

Finally, as  $K(t,s) \geq 0$  and

$$\int_{t_0}^t K(t,s) ds = \int_0^{t-t_0} \frac{1}{\tau} e^{-u/\tau} du \leq 1,$$

it follows that

$$\left| \tau^2 \int_{t_0}^t K(t,s) y''(s) ds \right| \leq \tau^2 M,$$

which produces the bound of the statement.  $\square$

With this lemma in place, the proposition describing the first-order behavior of Adam's moments can be established.

**Proposition A.2** (First-order behavior of  $\mathbf{m}$  and  $\mathbf{v}$ ). *Let  $I = [t_0, t_1]$  be a compact interval and let  $\mathbf{g} : I \rightarrow \mathbb{R}^d$  be a  $C^2$  mapping such that, for each coordinate  $i \in \{1, \dots, d\}$  one has that  $g_i(t) \neq 0$ , and set*

$$\Lambda := \sup_{t \in I} \max_{1 \leq i \leq d} |\delta_i(t)| \quad \text{and} \quad \Lambda' := \sup_{t \in I} \max_{1 \leq i \leq d} |\delta'_i(t)|.$$

*Let  $\mathbf{m}(t)$  and  $\mathbf{v}(t)$  solve the first two equations of the Adam flow (7) on  $I$ , with arbitrary initial conditions at  $t_0$ . Then, for each coordinate  $i$  and all  $t \in I$ ,*

$$\begin{aligned} m_i(t) &= g_i(t) \left( 1 - \tau_1 \delta_i(t) \right) + r_i^{(m)}(t), \\ v_i(t) &= g_i(t)^2 \left( 1 - 2\tau_2 \delta_i(t) \right) + r_i^{(v)}(t), \end{aligned}$$

*where the remainders  $r_i^{(m)}(t)$  and  $r_i^{(v)}(t)$  admit bounds of the form*

$$\begin{aligned} |r_i^{(m)}(t)| &\leq C_{m,i} \left( e^{-(t-t_0)/\tau_1} + \tau_1^2 (\Lambda^2 + \Lambda') \right), \\ |r_i^{(v)}(t)| &\leq C_{v,i} \left( e^{-(t-t_0)/\tau_2} + \tau_2^2 (\Lambda^2 + \Lambda') \right), \end{aligned}$$

*for some constants  $C_{m,i}, C_{v,i} > 0$  depending only on bounds on  $\mathbf{g}$  and on  $\tau_1, \tau_2$ . In particular, when  $t - t_0 \gg \max\{\tau_1, \tau_2\}$ , the transient factors  $e^{-(t-t_0)/\tau_i}$  have decayed, so that the remainders are uniformly of order  $\mathcal{O}(\Lambda^2 + \Lambda')$ , which agrees with the expansion in Proposition 3.2 in the main text.*

*Proof.* Since the dynamics decouples across coordinates, fix an index  $i$  and work on a single component, denoted by  $g(t)$ ,  $m(t)$ ,  $v(t)$  and  $\delta(t)$  to simplify notation.

*Step 1: expansion for  $m(t)$ .* The first equation of the Adam flow reads

$$\tau_1 m'(t) = -m(t) + g(t).$$

Applying Lemma A.1 with  $y(t) = g(t)$  and  $\tau = \tau_1$  yields

$$m(t) = g(t) - \tau_1 g'(t) + r_1(t),$$

where

$$|r_1(t)| \leq \left| m(t_0) - g(t_0) + \tau_1 g'(t_0) \right| e^{-(t-t_0)/\tau_1} + \tau_1^2 M_g,$$

and  $M_g := \sup_{t \in I} |g''(t)|$ .

By definition,  $\delta(t) = g'(t)/g(t)$ , hence

$$g'(t) = g(t) \delta(t) \quad \text{and} \quad g''(t) = (\delta(t)^2 + \delta'(t)) g(t).$$

Therefore,

$$M_g \leq \sup_{t \in I} |g(t)| (|\delta(t)|^2 + |\delta'(t)|) \leq B(\Lambda^2 + \Lambda'),$$

where  $B := \sup_{t \in I} |g(t)|$ . Substituting  $g'(t) = g(t)\delta(t)$  into the expression for  $m(t)$  gives

$$m(t) = g(t)(1 - \tau_1 \delta(t)) + r_1(t),$$

with

$$|r_1(t)| \leq \left| m(t_0) - g(t_0) + \tau_1 g(t_0) \delta(t_0) \right| e^{-(t-t_0)/\tau_1} + \tau_1^2 B(\Lambda^2 + \Lambda').$$

This has the stated form for  $m(t)$  with  $r^{(m)}(t) = r_1(t)$  and a bound of the desired type, upon taking

$$C_{m,i} := \left| m(t_0) - g(t_0) + \tau_1 g(t_0) \delta(t_0) \right| + B.$$

*Step 2: expansion for  $v(t)$ .* The second equation of the Adam flow is

$$\tau_2 v'(t) = -v(t) + g(t)^2.$$

Lemma A.1 applies again, now with  $y(t) = g(t)^2$  and  $\tau = \tau_2$ , yielding

$$v(t) = g(t)^2 - \tau_2 (g^2)'(t) + r_2(t),$$

where

$$|r_2(t)| \leq \left| v(t_0) - g(t_0)^2 + \tau_2 (g^2)'(t_0) \right| e^{-(t-t_0)/\tau_2} + \tau_2^2 M_{g^2},$$

and  $M_{g^2} := \sup_{t \in I} |(g^2)''(t)|$ . Since

$$(g^2)'(t) = 2g(t)g'(t),$$

it follows that

$$\begin{aligned} (g^2)''(t) &= 2(g'(t))^2 + 2g(t)g''(t) \\ &= 2g(t)^2 \delta(t)^2 + 2g(t)^2 (\delta'(t) + \delta(t)^2) \\ &= 2g(t)^2 (2\delta(t)^2 + \delta'(t)). \end{aligned}$$

Consequently, in terms of  $B = \sup_{t \in I} |g(t)|$ ,  $M_{g^2}$  is bounded by

$$M_{g^2} \leq 2B^2(2\Lambda^2 + \Lambda') \leq 4B^2(\Lambda^2 + \Lambda').$$

Substituting  $(g^2)'(t) = 2g(t)^2 \delta(t)$  into the expression for  $v(t)$  yields

$$v(t) = g(t)^2 (1 - 2\tau_2 \delta(t)) + r_2(t),$$

with

$$|r_2(t)| \leq \left| v(t_0) - g(t_0)^2 + 2\tau_2 g(t_0)^2 \delta(t_0) \right| e^{-(t-t_0)/\tau_2} + 4\tau_2^2 B^2(\Lambda^2 + \Lambda').$$

This gives a bound of the desired form for  $r^{(v)}(t) = r_2(t)$  by taking

$$C_{v,i} := \left| v(t_0) - g(t_0)^2 + 2\tau_2 g(t_0)^2 \delta(t_0) \right| + 4B^2,$$

and the result follows.  $\square$

The proposition above formalizes the heuristic in the main text: in a regime where the logarithmic drift  $\delta(t)$  is small and the exponential transients have decayed, the moments  $\mathbf{m}(t)$  and  $\mathbf{v}(t)$  track  $\mathbf{g}(t)$  and  $\mathbf{g}(t)^2$  up to first-order corrections proportional to  $\tau_1 \delta(t)$  and  $2\tau_2 \delta(t)$ , respectively, with errors controlled by  $\Lambda^2 + \Lambda'$ .

### A.3. First Order Expansion of the Normalized Update $\mathbf{R}(t)$

Building on the first-order expansions of  $\mathbf{m}(t)$  and  $\mathbf{v}(t)$  obtained in Proposition 3.2, we now derive a corresponding expansion for the normalized update

$$\mathbf{R}(t) := \frac{\mathbf{m}(t)}{\sqrt{\mathbf{v}(t)}}.$$

The goal is to make precise the informal statement in the main text that, in the regime of small logarithmic drift  $\delta(t)$ , the Adam update behaves like a sign-based method with a first-order correction proportional to  $(\tau_2 - \tau_1)\delta(t)$ .

**Theorem A.3** (First-order expansion of the normalized update). *Let  $I = [t_0, t_1]$  be a compact interval and let  $\mathbf{g} : I \rightarrow \mathbb{R}^d$  be a  $C^2$  mapping such that, for each coordinate  $i \in \{1, \dots, d\}$  one has that  $|g_i(t)| \geq g_{\min,i} > 0$  for all  $t \in I$ , and set*

$$\Lambda := \sup_{t \in I} \max_{1 \leq i \leq d} |\delta_i(t)| \quad \text{and} \quad \Lambda' := \sup_{t \in I} \max_{1 \leq i \leq d} |\delta'_i(t)|.$$

*Let  $\mathbf{m}(t)$  and  $\mathbf{v}(t)$  solve the first two equations of the Adam flow (7) on  $I$ , with arbitrary initial conditions at  $t_0$ . Then there exist constants  $C_{R,i} > 0$  and  $\varepsilon_0 > 0$ , depending only on bounds on  $\mathbf{g}$  and on  $\tau_1, \tau_2$ , such that, if  $\Lambda \leq \varepsilon_0$ , for each coordinate  $i$  and all  $t \in I$ ,*

$$R_i(t) = \text{sign}(g_i(t)) \left( 1 + (\tau_2 - \tau_1) \delta_i(t) \right) + \rho_i(t),$$

*with remainder bounded by*

$$|\rho_i(t)| \leq C_{R,i} \left( e^{-(t-t_0)/\tau_*} + \Lambda^2 + \Lambda' \right),$$

*with  $\tau_* := \max\{\tau_1, \tau_2\}$ . In particular, when  $t - t_0 \gg \tau_*$ , the transient factor  $e^{-(t-t_0)/\tau_*}$  has decayed, so that the deviation from the first-order expansion is uniformly of order  $\mathcal{O}(\Lambda^2 + \Lambda')$ , which agrees with Theorem 3.3 in the main text.*

*Proof.* Fix a coordinate index  $i$  and omit the subscript  $i$  from the notation: the scalar quantities associated with this coordinate are denoted by  $g(t)$ ,  $m(t)$ ,  $v(t)$ ,  $\delta(t)$ , and  $R(t)$ .

*Step 1:  $v(t)$  is bounded away from zero.* The variation-of-constants formula for  $\tau_2 v'(t) = -v(t) + g(t)^2$  yields, for all  $t \in I$ ,

$$v(t) = e^{-(t-t_0)/\tau_2} v(t_0) + \frac{1}{\tau_2} \int_{t_0}^t e^{-(t-s)/\tau_2} g(s)^2 ds.$$

As  $g(s)^2 \geq g_{\min}^2$  on  $I$ , it follows that

$$v(t) \geq e^{-(t-t_0)/\tau_2} v(t_0) + \frac{g_{\min}^2}{\tau_2} \int_{t_0}^t e^{-(t-s)/\tau_2} ds = g_{\min}^2 + e^{-(t-t_0)/\tau_2} (v(t_0) - g_{\min}^2).$$

In particular, once the transient factor  $e^{-(t-t_0)/\tau_2}$  is small enough,  $v(t) \geq \frac{1}{2}g_{\min}^2$ , so that  $\sqrt{v(t)}$  is well defined and bounded away from zero.

*Step 2: scalar expansions and normalization.* By Proposition A.2, for all  $t \in I$ ,

$$\begin{aligned} m(t) &= g(t) \left( 1 - \tau_1 \delta(t) \right) + r^{(m)}(t), \\ v(t) &= g(t)^2 \left( 1 - 2\tau_2 \delta(t) \right) + r^{(v)}(t), \end{aligned} \tag{9}$$

with remainders satisfying

$$\begin{aligned} |r^{(m)}(t)| &\leq C_m \left( e^{-(t-t_0)/\tau_1} + \tau_1^2 (\Lambda^2 + \Lambda') \right), \\ |r^{(v)}(t)| &\leq C_v \left( e^{-(t-t_0)/\tau_2} + \tau_2^2 (\Lambda^2 + \Lambda') \right), \end{aligned} \tag{10}$$

for some constants  $C_m, C_v > 0$ . Since  $g$  is continuous and nonvanishing on  $I$ , the quantity  $\text{sign}(g(t))$  is constant on  $I$ . Using (9), write

$$m(t) = g(t)(1 + b(t)), \quad v(t) = g(t)^2(1 + a(t)),$$

where

$$b(t) := -\tau_1 \delta(t) + \frac{r^{(m)}(t)}{g(t)}, \quad a(t) := -2\tau_2 \delta(t) + \frac{r^{(v)}(t)}{g(t)^2}.$$

Then

$$R(t) = \frac{m(t)}{\sqrt{v(t)}} = \frac{g(t)(1+b(t))}{|g(t)|\sqrt{1+a(t)}} = \text{sign}(g(t)) \frac{1+b(t)}{\sqrt{1+a(t)}}.$$

*Step 3: control of  $a(t)$  and  $b(t)$ .* From (10) and the lower and upper bounds on  $g(t)$ , there exist constants  $C_a, C_b > 0$  such that, for all  $t \in I$ ,

$$\begin{aligned} |b(t)| &\leq C_b \left( |\delta(t)| + e^{-(t-t_0)/\tau_1} + \Lambda^2 + \Lambda' \right), \\ |a(t)| &\leq C_a \left( |\delta(t)| + e^{-(t-t_0)/\tau_2} + \Lambda^2 + \Lambda' \right). \end{aligned} \tag{11}$$

*Step 4: expansion of  $(1+a(t))^{-1/2}$ .* In order to expand  $(1+a(t))^{-1/2}$ , it suffices to ensure that  $|a(t)| < \alpha < 1$ . Starting from the variation of constants formula for  $v(t)$  and bounding  $g_{\min} \leq |g(t)| \leq g_{\max}$  on  $I$ , it follows that

$$|a(t)| = \left| \frac{v(t)}{g(t)^2} - 1 \right| \leq \frac{g_{\max}^2}{g_{\min}^2} - 1 + e^{-(t-t_0)/\tau_2} \frac{|v(t_0) - g_{\max}^2|}{g_{\min}^2}.$$

It remains to relate  $g_{\max}/g_{\min}$  to  $\Lambda$ . Since  $\delta(t) = (\log |g(t)|)'$  and  $|\delta(t)| \leq \Lambda$  on  $I$  by definition, small  $\Lambda$  implies that  $\log |g(t)|$  varies little across  $I$ , and hence  $\log g_{\max} - \log g_{\min}$  can be made arbitrarily small. In particular,  $g_{\max}/g_{\min}$  can be made arbitrarily close to 1 by taking  $\Lambda$  sufficiently small. Plugged into the bound above, this shows that, for  $\Lambda$  small enough and once the transient term has decayed, one has  $|a(t)| \leq \alpha$  for some fixed  $\alpha \in (0, 1)$  on the time range under consideration.

Now consider  $\phi(u) = (1+u)^{-1/2}$  for  $|u| < 1$ . A Taylor expansion at  $u = 0$  yields

$$\phi(u) = 1 - \frac{1}{2}u + \psi(u),$$

where the remainder satisfies that  $|\psi(u)| \leq C_\phi u^2$  for all  $|u| \leq \alpha$ , for some constant  $C_\phi$  depending only on  $\alpha$ . With  $u = a(t)$ , one has that

$$\frac{1}{\sqrt{1+a(t)}} = 1 - \frac{1}{2}a(t) + \psi(a(t)),$$

where  $|\psi(a(t))| \leq C_\phi |a(t)|^2$ .

*Step 5: expansion of  $R(t)$  and remainder bounds.* In terms of the above expression, it follows that

$$\frac{1+b(t)}{\sqrt{1+a(t)}} = (1+b(t)) \left( 1 - \frac{1}{2}a(t) + \psi(a(t)) \right) = 1 + b(t) - \frac{1}{2}a(t) + \rho_0(t),$$

where

$$\rho_0(t) := -\frac{1}{2}b(t)a(t) + (1+b(t))\psi(a(t)).$$

Taking absolute values and using the bounds on  $a(t)$ ,  $b(t)$ , and  $\psi(a(t))$ , there exists a constant  $C_\rho > 0$  such that

$$|\rho_0(t)| \leq C_\rho \left( |b(t)| |a(t)| + |a(t)|^2 \right).$$

The bounds on (11) and the fact that  $|\delta(t)| \leq \Lambda$  for all  $t \in I$  imply that there exists  $C'_\rho > 0$  with

$$|\rho_0(t)| \leq C'_\rho \left( e^{-(t-t_0)/\tau_*} + \Lambda^2 + \Lambda' \right), \quad \tau_* := \max\{\tau_1, \tau_2\}. \tag{12}$$

Moreover, the linear part in  $a(t)$  and  $b(t)$  can be written explicitly in terms of  $\delta(t)$  and the remainders  $r^{(m)}(t)$  and  $r^{(v)}(t)$  as

$$b(t) - \frac{1}{2}a(t) = \left( -\tau_1 \delta(t) + \frac{1}{2} \cdot 2\tau_2 \delta(t) \right) + \left( \frac{r^{(m)}(t)}{g(t)} - \frac{1}{2} \frac{r^{(v)}(t)}{g(t)^2} \right) = (\tau_2 - \tau_1) \delta(t) + \tilde{r}(t),$$

where

$$\tilde{r}(t) := \frac{r^{(m)}(t)}{g(t)} - \frac{1}{2} \frac{r^{(v)}(t)}{g(t)^2}.$$

Now, the bounds on (10) and the upper and lower bounds on  $g(t)$  force the existence of a constant  $C_{\tilde{r}} > 0$  such that

$$|\tilde{r}(t)| \leq C_{\tilde{r}} \left( e^{-(t-t_0)/\tau_*} + \Lambda^2 + \Lambda' \right).$$

Combining the previous identities gives

$$\frac{1+b(t)}{\sqrt{1+a(t)}} = 1 + (\tau_2 - \tau_1)\delta(t) + \tilde{r}(t) + \rho_0(t).$$

Defining  $\rho(t) := \tilde{r}(t) + \rho_0(t)$ , the bounds for  $\tilde{r}(t)$  and  $\rho_0(t)$  imply that there exists a constant  $C_R > 0$  (for instance  $C_R := C_{\tilde{r}} + C'_\rho$ ) such that

$$|\rho(t)| \leq C_R \left( e^{-(t-t_0)/\tau_*} + \Lambda^2 + \Lambda' \right).$$

Finally, recall that

$$R(t) = \text{sign}(g(t)) \frac{1+b(t)}{\sqrt{1+a(t)}},$$

so the previous expansion yields

$$R(t) = \text{sign}(g(t)) \left( 1 + (\tau_2 - \tau_1)\delta(t) \right) + \text{sign}(g(t)) \rho(t).$$

Setting  $\rho_i(t) := \text{sign}(g(t)) \rho(t)$  and absorbing the sign into the constant gives the desired form with the prescribed bound for the fixed coordinate  $i$ , and hence the result follows.  $\square$

Theorem A.3 provides the rigorous justification for the informal expansion used in the main text: in the regime of small logarithmic drift and after the transient has decayed, the normalized update of the Adam flow behaves like a sign-based method with a first-order sensitivity to scale drift controlled by  $\tau_2 - \tau_1$ , and with higher-order corrections of size  $\mathcal{O}(\Lambda^2 + \Lambda')$ .

In what follows, briefly comments on how the above analysis extends to the more standard practical variant of Adam that uses bias correction and a nonzero stabilisation constant  $\varepsilon > 0$  are provided.

*Remark A.4* (Bias correction). In discrete time, Adam is often implemented with bias-corrected moments,

$$\hat{\mathbf{m}}_{k+1} = \frac{\mathbf{m}_{k+1}}{1 - \beta_1^{k+1}}, \quad \hat{\mathbf{v}}_{k+1} = \frac{\mathbf{v}_{k+1}}{1 - \beta_2^{k+1}},$$

and the update

$$\boldsymbol{\theta}_{k+1} = \boldsymbol{\theta}_k - \eta \frac{\hat{\mathbf{m}}_{k+1}}{\sqrt{\hat{\mathbf{v}}_{k+1}} + \varepsilon}.$$

The correction factors  $(1 - \beta_1^{k+1})^{-1}$  and  $(1 - \beta_2^{k+1})^{-1}$  converge exponentially fast to 1 as  $k \rightarrow \infty$  at rates controlled by  $(1 - \beta_1)$  and  $(1 - \beta_2)$ . In particular, on time scales comparable with the relaxation times  $\tau_1$  and  $\tau_2$ , they only affect the dynamics through an initial transient which decays exponentially.

When passing to the continuous-time limit, the bias-corrected and uncorrected recurrences therefore give rise to the *same* limiting flow (7), up to a choice of initial condition for  $\mathbf{m}(t)$  and  $\mathbf{v}(t)$  that accounts for the finite-time bias. All the expansions in Proposition 3.2 and Theorem 3.3 are stable under such changes of initial data, since the only place where initial conditions enter is through the exponentially decaying terms of the form  $\exp(-t-t_0/\tau_1)$  and  $\exp(-t-t_0/\tau_2)$  already present in the bounds. In particular, the structure of the first-order term  $(\tau_2 - \tau_1)\delta_i(t)$  and the scale invariance considerations are unchanged by bias correction.

*Remark A.5* (Nonzero  $\varepsilon$ ). If we keep  $\varepsilon > 0$  in the denominator, the normalized update in continuous time becomes

$$R_{\varepsilon,i}(t) := \frac{m_i(t)}{\sqrt{v_i(t)} + \varepsilon}$$

for each coordinate  $i$ . The expansions for  $m_i(t)$  and  $v_i(t)$  in Proposition 3.2 remain valid, so we can write

$$R_{\varepsilon,i}(t) = \frac{m_i(t)}{\sqrt{v_i(t)}} \left(1 + \frac{\varepsilon}{\sqrt{v_i(t)}}\right)^{-1}.$$

Under the hypotheses of Theorem 3.3,  $|g_i(t)|$  is bounded below by  $g_{\min,i} > 0$ , and the expansion of Proposition A.2 implies that  $\sqrt{v_i(t)}$  is uniformly comparable to  $|g_i(t)|$ . A Taylor expansion of  $(1+u)^{-1}$  at  $u=0$  then shows that

$$R_{\varepsilon,i}(t) = R_i(t) + \kappa_i(t),$$

where  $R_i(t)$  is the update without  $\varepsilon$  and

$$|\kappa_i(t)| \leq C_{\varepsilon,i} \frac{\varepsilon}{|g_i(t)|} + \text{higher-order terms in } \frac{\varepsilon}{|g_i(t)|},$$

for some constant  $C_{\varepsilon,i} > 0$  depending only on the same bounds as in Theorem 3.3. In particular, combining this with the main equation of Theorem A.3 yields

$$R_{\varepsilon,i}(t) = \text{sign}(g_i(t)) \left(1 + (\tau_2 - \tau_1)\delta_i(t)\right) + \rho_i(t) + \kappa_i(t),$$

with  $\rho_i(t)$  bounded as in Theorem A.3 and  $|\kappa_i(t)| \lesssim \varepsilon/|g_i(t)|$ .

Thus, as long as  $\varepsilon$  is small compared to the typical magnitude of the gradients (for example  $\varepsilon \ll \min_{t \in I, i} |g_i(t)|$  along the trajectory segment under consideration), the additional contribution  $\kappa_i(t)$  is dominated by the  $\mathcal{O}(\Lambda^2 + \Lambda')$  term in Theorem 3.3, and the first-order scale invariance discussion in the main text applies unchanged. On the other hand, if  $\varepsilon$  is taken large relative to  $|g_i(t)|$ , the ratio  $\varepsilon/|g_i(t)|$  can be of order one or larger, and the denominator  $\sqrt{v_i(t)} + \varepsilon$  becomes dominated by  $\varepsilon$ . In that regime the update is effectively controlled by the absolute scale set by  $\varepsilon$ , and the scale invariance properties of the idealized flow are no longer a good approximation of the discrete algorithm.

## B. Additional Experiments

### B.1. Additional Training Dynamics

In this section, we report the training dynamics for the five remaining network–dataset pairs considered in our study. These results are relegated to the appendix due to space constraints, but follow exactly the same experimental protocol and visualization format as the examples presented in the main body of the paper.

In all figures, we show the training dynamics for the corresponding model and dataset. Each panel displays the evolution of the training loss (left axis) and the norm of the update  $\mathbf{R}_k$  (right axis) for a fixed pair  $(\beta_1, \beta_2)$ . Rows correspond to fixed values of  $\beta_1$ , while columns vary  $\beta_2$ , with identical axis scales within each row to enable direct comparison. Curves represent the seed-averaged dynamics after exponential smoothing with a window of 200 steps, and shaded regions indicate one standard deviation across random seeds. The oscillation metric  $\omega$ , reported in the title of each panel, is computed as the mean across seeds for the corresponding pair  $(\beta_1, \beta_2)$ .

Across all configurations, the qualitative behavior observed in these figures closely mirrors that reported in the main text. In particular, when comparing panels row-wise, configurations along the diagonal  $\beta_1 = \beta_2$  consistently exhibit smoother update norms and reduced oscillatory behavior, while off-diagonal choices lead to visibly larger fluctuations. This visual consistency across architectures and datasets further supports the generality of the phenomenon highlighted in the main experiments.

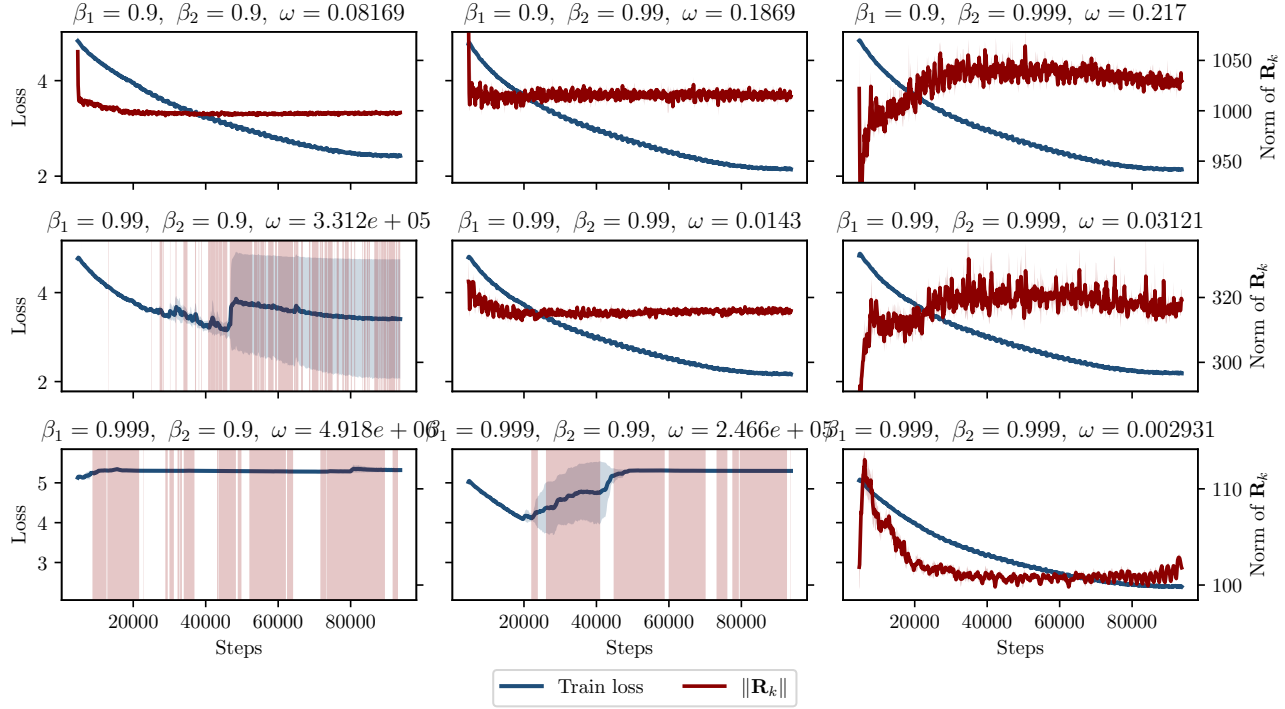


Figure 4. Training dynamics for EfficientNet-B0 on TinyImageNet.

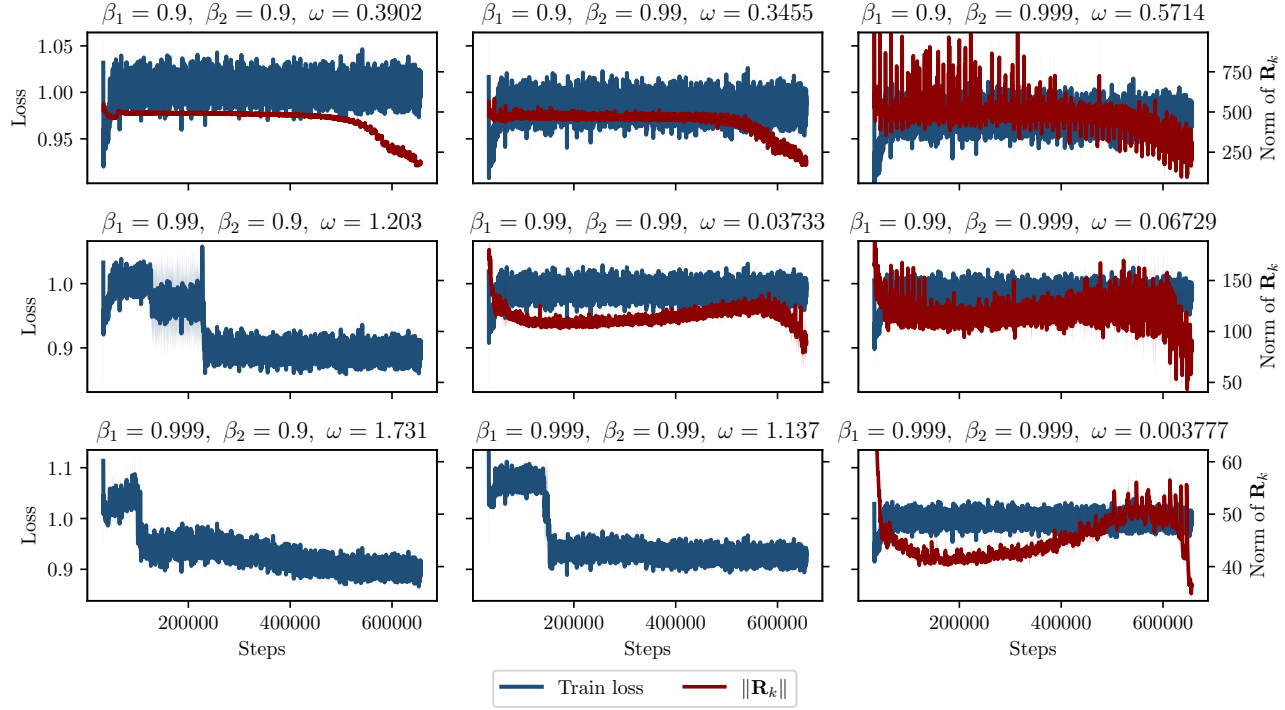


Figure 5. Training dynamics for T5 on SQuAD.

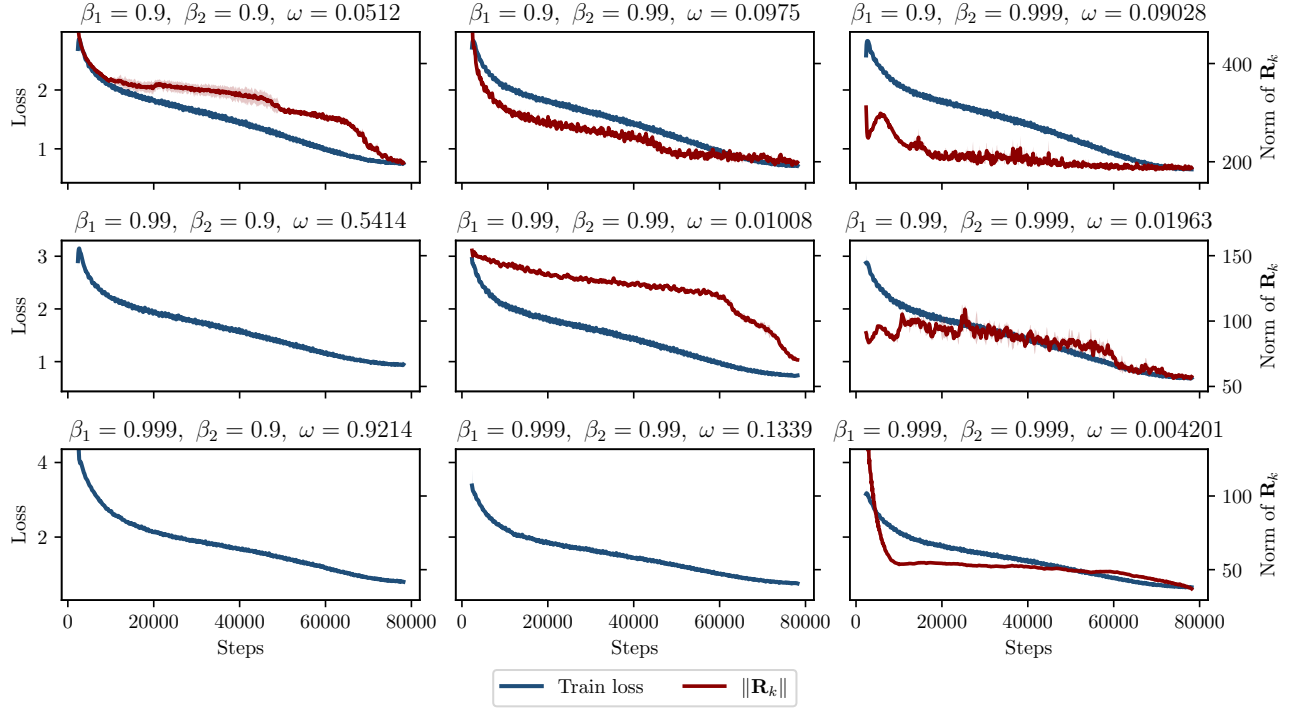


Figure 6. Training dynamics for ResNet18 on CIFAR-100.

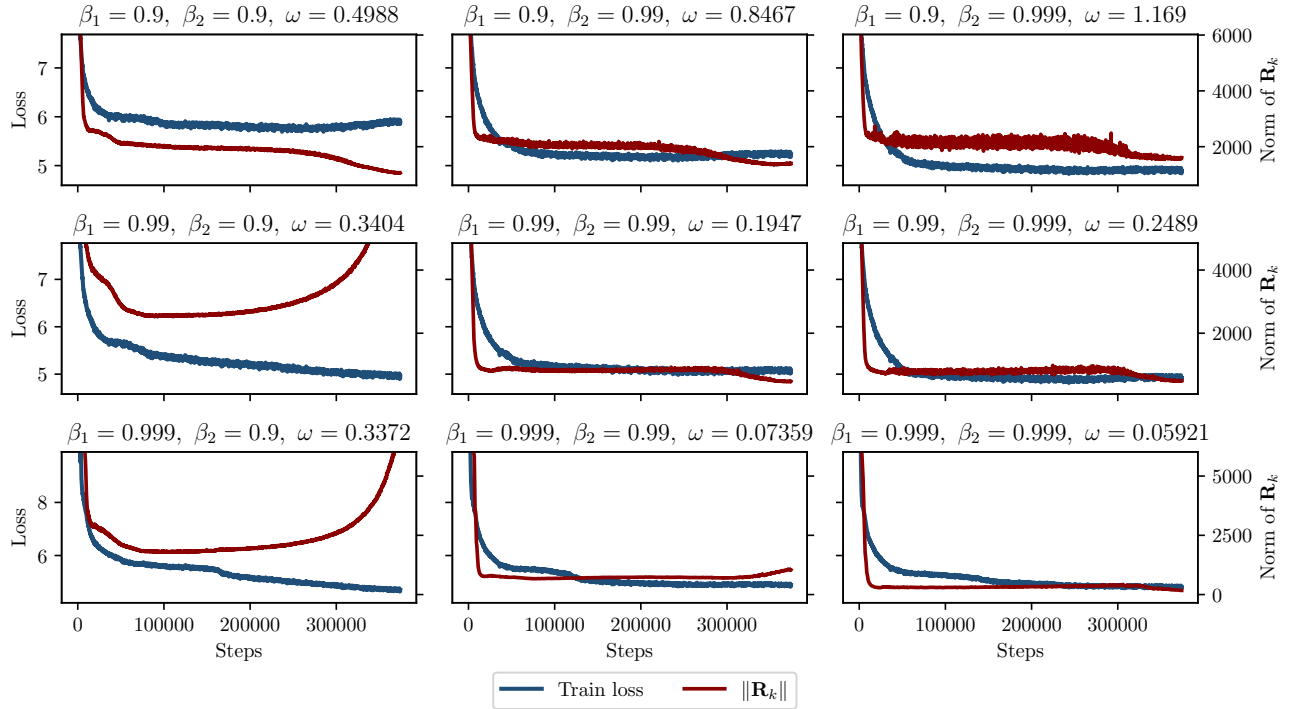


Figure 7. Training dynamics for NanoGPT on SlimPajama.

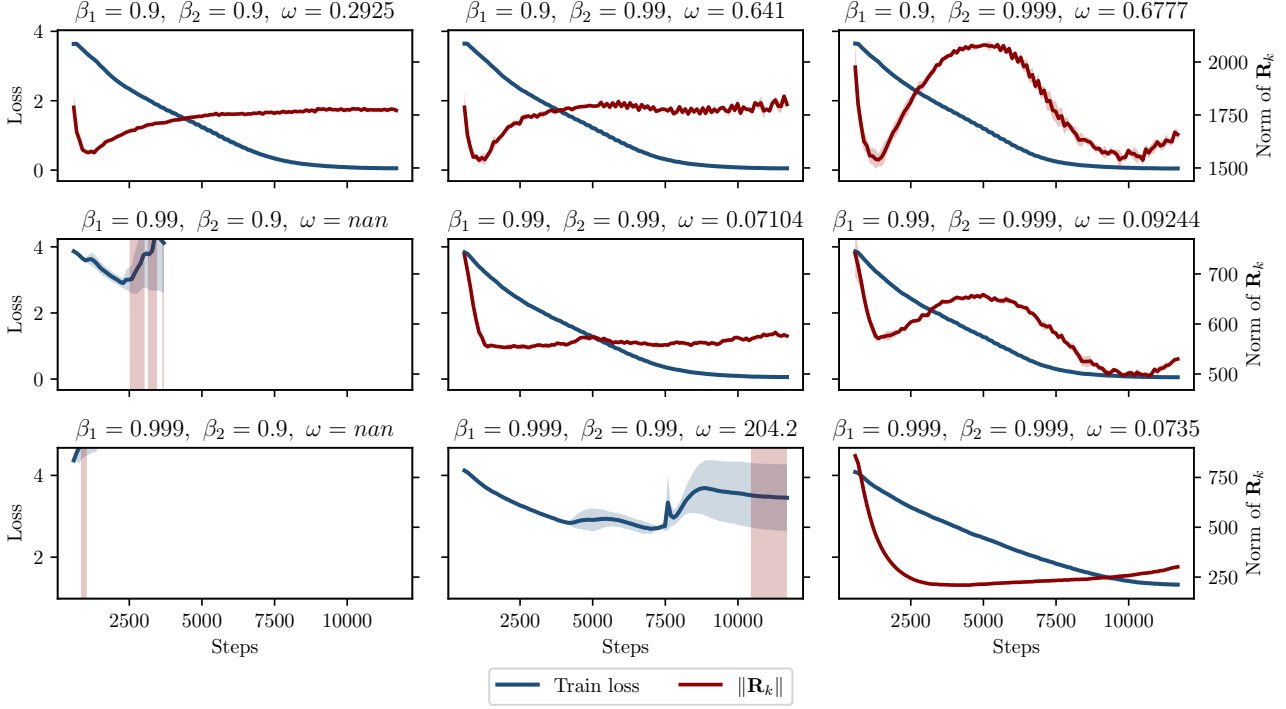


Figure 8. Training dynamics for ViT-B16 on CIFAR-100.

## B.2. Ablation on the Oscillation Metric and Smoothing Window

We further assess the robustness of our conclusions with respect to both the definition of the oscillation metric and the choice of the smoothing window. In the main experiments, oscillation is quantified using a first-order metric, denoted by  $\omega_1$  ( $\omega$  in the main text), which measures the average magnitude of consecutive variations in the update norm. Given the smoothed sequence  $\{x_k\}_{k=1}^T$  derived from a EMA of the sequence  $\|\mathbf{R}_k\|$ , this metric is defined as

$$\omega_1(x) = \frac{1}{T-1} \sum_{k=1}^{T-1} |x_{k+1} - x_k|,$$

capturing the typical step-to-step variation of the update magnitude.

In addition, we consider an alternative second-order metric, denoted by  $\omega_2$ , based on discrete second differences. This metric measures the overall magnitude of curvature in the sequence  $\{x_k\}$  and is sensitive to higher-frequency fluctuations. Concretely, we set

$$\omega_2(x) = \frac{1}{T-1} \sum_{k=1}^{T-1} |x_{k+1} - 2x_k + x_{k-1}|,$$

with suitable one-sided differences at the boundaries. While  $\omega_1$  directly reflects local variability,  $\omega_2$  captures rapid changes in slope and emphasizes oscillatory behavior at shorter time scales.

For both metrics, we vary the exponential smoothing window over the set  $\{1, 10, 100, 200, 500\}$  and, for each configuration, repeat the same statistical test described in the main text. For brevity, we do not report the raw oscillation values; instead, we summarize the results in terms of the selection rate of the diagonal  $\beta_1 = \beta_2$  and the corresponding one-sided binomial  $p$ -values, reported in Table 2.

Focusing first on  $\omega_1$ , the metric used throughout the main article, we observe that the results are stable for sufficiently large windows, with  $p$ -values consistently below 0.05 once  $w \geq 100$  in most settings. For smaller windows, the oscillation signal becomes partially obscured by stochastic fluctuations inherent to minibatch training, leading to weaker statistical significance despite unchanged underlying trends.

Table 2. Ablation results for the smoothing window and the oscillation metric. For each experiment and window size, we report the rate at which the diagonal  $\beta_1 = \beta_2$  minimizes the oscillation, together with the corresponding one-sided exact binomial test  $p$ -value. Results are shown for the first-order metric  $\omega_1$ , based on absolute first differences of the smoothed  $\|\mathbf{R}_k\|$ , and for the second-order metric  $\omega_2$ , based on discrete second differences.

Exp.	Model	Dataset	Window	$\omega_1$		$\omega_2$	
				Rate	$p$ -value	Rate	$p$ -value
1	NanoGPT	SlimPajama	1	100%	0.037037	100%	0.037037
			10	67%	0.259259	100%	0.037037
			100	100%	0.037037	100%	0.037037
			200	100%	0.037037	100%	0.037037
			500	100%	0.037037	100%	0.037037
2	EfficientNet-B0	TinyImageNet	1	100%	$5.08 \times 10^{-5}$	100%	$5.08 \times 10^{-5}$
			10	100%	$5.08 \times 10^{-5}$	100%	$5.08 \times 10^{-5}$
			100	100%	$5.08 \times 10^{-5}$	100%	$5.08 \times 10^{-5}$
			200	100%	$5.08 \times 10^{-5}$	100%	$5.08 \times 10^{-5}$
			500	100%	$5.08 \times 10^{-5}$	100%	$5.08 \times 10^{-5}$
3	T5	SQuAD	1	67%	0.042422	56%	0.144846
			10	67%	0.042422	67%	0.042422
			100	67%	0.042422	67%	0.042422
			200	78%	0.008281	67%	0.042422
			500	78%	0.008281	67%	0.042422
4	ResNet18	CIFAR-100	1	50%	0.054402	75%	0.000392
			10	75%	0.000392	50%	0.054402
			100	75%	0.000392	50%	0.054402
			200	75%	0.000392	50%	0.054402
			500	75%	0.000392	50%	0.054402
5	NanoGPT	WikiText	1	56%	0.144846	56%	0.144846
			10	44%	0.349693	67%	0.042422
			100	89%	0.000965	44%	0.349693
			200	100%	$5.08 \times 10^{-5}$	56%	0.144846
			500	100%	$5.08 \times 10^{-5}$	56%	0.144846
6	ViT-B16	CIFAR-100	1	100%	$5.08 \times 10^{-5}$	100%	$5.08 \times 10^{-5}$
			10	100%	$5.08 \times 10^{-5}$	100%	$5.08 \times 10^{-5}$
			100	100%	$5.08 \times 10^{-5}$	100%	$5.08 \times 10^{-5}$
			200	100%	$5.08 \times 10^{-5}$	100%	$5.08 \times 10^{-5}$
			500	100%	$5.08 \times 10^{-5}$	100%	$5.08 \times 10^{-5}$

For the second-order metric  $\omega_2$ , the diagonal  $\beta_1 = \beta_2$  is again favored across experiments, with  $p$ -values typically below or close to the 0.05 threshold for  $w \geq 10$ . However, the corresponding selection rates are generally comparable to, and in some cases slightly lower than, those obtained with  $\omega_1$ . This suggests that while second-order differences capture complementary aspects of oscillatory behavior, the simpler first-order metric provides a more direct and robust characterization of update stability in this setting.

## C. Implementation Details

**Common setup.** All experiments evaluated Adam-type optimizers over a  $3 \times 3$  momentum grid  $(\beta_1, \beta_2) \in \{0.9, 0.99, 0.999\}^2$ . Models were initialized using the same sinusoidal scheme (Fernández-Hernández et al., 2025) for accelerating training and trained in full FP32 precision, disabling both mixed precision and TF32 operations. Whenever specified, random seeds were fixed for NumPy and PyTorch. Learning rates followed a linear warm-up phase up to the base value, followed by cosine annealing for the remainder of training using SequentialLR.

**Experiment 1 (NanoGPT, SlimPajama).** Training employed Adam with base learning rate  $3 \times 10^{-4}$  and weight decay  $10^{-4}$  for one epoch. Warm-up covered 20% of the total training steps, starting from a factor  $10^{-2}$  of the base learning rate. Gradient clipping with maximum norm 1 was enabled. The model followed a GPT-2 small configuration with 12 layers, 12 attention heads, hidden size 768, block size 1024, dropout 0.1, and bias terms enabled.

**Experiment 2 (EfficientNet-B0, TinyImageNet).** Optimization relied on AdamW with learning rate  $10^{-3}$  and weight decay  $3 \times 10^{-5}$  over 60 epochs. Warm-up spanned 20% of the training epochs, starting from a factor  $10^{-1}$ . The classifier head was replaced by a dropout layer with rate 0.6 followed by a linear projection to 200 classes. Training used cross-entropy loss with label smoothing 0.1.

**Experiment 3 (T5, SQuAD).** Adam was used with learning rate  $10^{-3}$  and weight decay  $10^{-2}$  for 60 epochs. Warm-up lasted 20% of epochs, starting from a factor  $10^{-2}$ . Training minimized the model-provided cross-entropy loss returned by the forward pass.

**Experiment 4 (ResNet18, CIFAR-100).** Training employed Adam with learning rate  $2 \times 10^{-2}$  and weight decay  $10^{-3}$  over 100 epochs while sweeping all  $(\beta_1, \beta_2)$  combinations. Warm-up was applied over the first 10 epochs, starting from a factor 0.1 of the base learning rate. Standard cross-entropy loss was used.

**Experiment 5 (NanoGPT, WikiText-2).** Adam with learning rate  $3 \times 10^{-4}$  and weight decay  $10^{-4}$  was used for 60 epochs. Warm-up covered 20% of training steps, starting from a factor  $10^{-2}$ . Gradient clipping with norm 1 was enabled. The architecture matched GPT-2 small (12 layers, 12 heads, hidden size 768, block size 1024, dropout 0.1). Training used WikiText-2 with batch size 8, block size 256, and GPT-2 tokenization.

**Experiment 6 (ViT-B16, CIFAR-100).** Optimization employed AdamW with learning rate  $3 \times 10^{-4}$  and weight decay 0.2 over 60 epochs. Warm-up spanned 10% of epochs, starting from a factor 0.1. Cross-entropy loss was used. Non-finite losses triggered skipped updates, and non-finite gradients and optimizer states were sanitized via `nan_to_num`.

**Hardware.** All experiments were executed on a multi-GPU server equipped with NVIDIA A100-SXM4 GPUs with 80 GB of HBM2 memory each. Training runs typically utilized up to three GPUs concurrently, each operating at full utilization during active workloads. The host system featured dual AMD EPYC 7513 processors (64 physical cores in total) with a NUMA architecture across eight nodes. All computations were performed under x86\_64 Linux in full FP32 precision.